Egyptian Journal of Chemistry

http://ejchem.journals.ekb.eg/

Bioactive Hydrogel-Coated Fabric Dressings Based on Chemically Modified Biopolymers and Plant-Derived Silver Nanoparticles for Enhanced Pressure Ulcer Healing

Aya Sediek [a], Mohamed M. Mosaad [a], Hanan A. Othman [a], and Amina L. Mohamed [b]*

[a] *Textile Printing, Dyeing and Finishing Department, Faculty of Applied Arts, Benha University, Benha, Egypt*

[b] *National Research Centre (Scopus affiliation ID 60014618), Textile Research and Technology Institute, Pre-treatment, and Finishing of Cellulose-based Textiles Department, 33 El-Behouth St. (former El-Tahrir str.), Dokki, P.O 12622, Giza, Egypt*

In Loving Memory of Late Professor Doctor"" Issa Mohammed Imam Fakhr""

Abstract

In this study, a bioactive hydrogel-coated textile dressing was developed for potential application in pressure ulcer management. The hydrogel matrix was formed via Schiff base crosslinking between O-carboxymethyl chitosan (O-CMC) and oxidised sodium alginate (Ox-NaAlg). O-CMC was synthesised through controlled carboxymethylation of chitosan, while Ox-NaAlg was prepared by periodate oxidation to introduce reactive aldehyde groups. Plant-derived extracts of Hypericum perforatum and Matricaria chamomilla were incorporated into the hydrogel system, either directly or as reducing agents for the green synthesis of silver nanoparticles (AgNPs). The resulting hydrogels were coated onto nonwoven cotton fabrics prior to complete gelation. Structural and physicochemical characterisation was performed using FTIR spectroscopy, UV–Vis spectroscopy, TEM, SEM, swelling studies, gelation time measurements, protein adsorption, and antioxidant activity assays. The results demonstrate successful hydrogel formation, stable incorporation of bioactive components, and tunable physicochemical properties depending on formulation composition. The developed hydrogel-coated fabrics exhibited characteristics suitable for wound dressing applications, including high water uptake, controlled protein interaction, and antioxidant potential. These findings indicate that the proposed system represents a promising platform for advanced wound care, warranting further biological validation.

Keywords: Pressure ulcer dressing; Bioactive hydrogel; O-carboxymethyl chitosan; Oxidised alginate; Plant-mediated silver nanoparticles; Nonwoven cotton fabric; Antibacterial and antioxidant properties; Cytocompatibility; Wound healing biomaterials

1. Introduction

Skin is the body's largest organ and acts as the primary line of defense, yet it is prone to damage, leading to skin wounds [1]. Pressure ulcers are a form of skin wounds, commonly known as bedsores, decubitus ulcers, or pressure injuries, and are localised areas of damage to the skin and/or underlying tissues. They generally occur due to sustained pressure or friction between soft tissue and bony prominences, leading to compromised blood flow and tissue damage [2-4].

The healing process of these wounds is influenced by factors such as the wound's size, depth, and the extent of damage to various skin layers, and typically, healing takes place relatively quickly with these factors. The literature consistently demonstrates that wound healing occurs more rapidly in covered wounds compared to uncovered ones. This accelerated healing is attributed to the protective properties of the dressing, including thermal, mechanical, and microbial insulation. Additionally, the regular application of medical bandages can significantly accelerate the healing process. Therefore, selecting the appropriate dressing is essential to promote faster healing and minimise the risk of microbial infections [5-7].

Traditional dressing options, such as bandages, gauze, and cotton pads, often lack effectiveness in promoting healing, relieving pain, and maintaining a moist environment for wound recovery. As a result, they frequently lead to slower healing, negatively impacting the overall wound repair process[8]. Additionally, these dressings may contribute to toxicity by promoting the growth of bacteria and other microorganisms [9].

* Corresponding author: alo.mohamed12@hotmail.com (AminaL. Mohamed)
Receive Date: 20 January 2026, Revise Date: 16 February 2026, Accept Date: 14 March 2026
DOI: 10.21608/ejchem.2026.461583.12943
©2026 National Information and Documentation Center (NIDOC)

Motivated by environmental and healthcare requirements, textile research has progressed from sustainable processing to sophisticated biomedical applications. Preliminary research [10-40] presented bio-based materials and environmentally friendly finishing technologies [14, 30, 34], whereas contemporary advancements integrate nanotechnology and intelligent composites, including phase change materials (PCMs) [27], polymer–clay systems [32], and nanoparticle applications [31, 35]. These improvements have facilitated the development of functional medical textiles, such as drug-delivery wound dressings and controlled-release biopolymer fabrics, underpinned by sustainable printing and circular material utilization. Thus, chemically modified biopolymers integrated with plant-derived silver nanoparticles present intriguing platforms for bioactive hydrogel-coated fabric dressings intended to expedite pressure ulcer healing [41-57].

Therefore, it is imperative to design novel dressings with multifunctional applications and improved efficacy. Recently, innovative formulations for advanced wound dressings have been investigated, aiming to enhance wound healing, facilitate controlled drug release, and enable targeted delivery to the wound site [58].

Over the past decade, the use of hydrogel-based wound dressings has grown significantly. These hydrogels are polymers featuring a 3D cross-linked structure, containing up to 90% water. This high-water content gives them a soft, comfortable feel while providing excellent water absorption and retention. Thanks to these unique properties, hydrogels are highly effective in wound care, as they maintain the moist environment essential for healing, absorb excess exudate, and accelerate the recovery process [59].

Hydrogels derived from sustainable and natural polymers are considered more suitable for biomedical applications than synthetic polymers due to their remarkable properties. These include their abundant availability, cost-effectiveness, and water absorption capabilities, which help maintain a moist environment conducive to wound healing. Additionally, they exhibit non-cytotoxicity, excellent biocompatibility, and biodegradability. Their semi-crystalline structures and varying levels of porosity, ranging from nano to macro-scale, enable them to effectively incorporate, bind, and release different amounts of active compounds, depending on their specific structural and physicochemical characteristics [60].

Chitosan, a deacetylated derivative of chitin, is known for its remarkable properties, including biocompatibility, biodegradability, antimicrobial activity, hemostasis, and cell adhesion. These characteristics make it vital in wound healing, as it supports tissue repair, neovascularisation, and dermal regeneration, while exhibiting analgesic, antimicrobial, and haemostatic effects. Chitosan can also form complex, multilayered hydrogels, improving outcomes in drug delivery, tissue engineering, and cell culture applications. Recently, Carboxymethyl-chitosan (CMC), a water-soluble derivative of chitosan containing both carboxyl and amino groups, has gained attention due to its superior solubility, enhanced antibacterial properties, and improved biocompatibility and safety for humans. The hydroxyl and amino groups in its polymer chain contribute to its antioxidant activity through free radical scavenging. These properties, along with their ability to bind bile acids, have been well documented. The molecular weight and functional groups in CMC also influence its antioxidant activity, making it a promising candidate for various biomedical, pharmaceutical, and environmental applications [61-64].

Alginate, a natural polysaccharide polymer extracted from marine brown algae, is a widely available and renewable material. Its use in wound dressings is attributed to its ability to maintain a moist environment and reduce bacterial contamination. Alginates stimulate immune cells, including macrophages and monocytes, to produce inflammatory cytokines such as IL-6 and TNF-α, which play a key role in accelerating wound healing. However, due to its hydrophilic nature, driven by the presence of numerous carboxyl and hydroxyl groups, alginate experiences uncontrolled degradation and excessive swelling, which compromises its stability in biological buffers and limits its biomedical applications. Notably, the oxidation of alginate improves its biodegradability and decreases its molecular weight. Oxidised alginate (OA), also known as alginate dialdehyde (ADA), is produced by oxidising sodium alginate, typically with periodate as the oxidising agent. Due to its high dialdehyde group reactivity and superior biocompatibility, oxidised sodium alginate is extensively utilised in tissue engineering applications to produce films, hydrogels, and beads [65-68].

Herbal treatments may present a viable alternative approach for the healing of pressure ulcers, offering potential therapeutic benefits [69]. Hypericum perforatum (commonly known as St. John's Wort) is a widely recognised medicinal plant with a long history of use in traditional dermatological practices. It has been employed in the treatment of various skin conditions, including minor wounds, cuts, burns, abrasions, bruises, and ulcers. The therapeutic effects of this plant have been substantiated by both in vitro and in vivo research, demonstrating its potential efficacy in promoting wound healing and alleviating skin-related ailments [70-72]. The therapeutic efficacy of Hypericum perforatum L. (Hypericaceae) in wound healing may be attributed to its antimicrobial and anti-inflammatory properties, alongside its ability to enhance fibroblast mobility, promote collagen synthesis, and support keratinocyte differentiation [73, 74].

Chamomile (Matricaria chamomilla) is a widely recognised herb known for its therapeutic effects on inflammation, infection, pain, and ulceration. It is commonly used for its sedative, anti-inflammatory, and spasmolytic properties, and is also effective in treating skin conditions such as psoriasis, eczema, and acne, as well as symptoms of fever and respiratory issues. Scientific studies have revealed that chamomile contains bioactive compounds, including chamazulene, alpha-bisabolol, bisabolol oxides, spiroethers, and flavonoids, which contribute to its anti-inflammatory, antibacterial, and antifungal properties. Notably, chamomile has demonstrated significant efficacy in promoting the healing of ulcers in non-diabetic rats. When applied topically, chamomile accelerates burn wound healing by enhancing reepithelialisation, stimulating fibroblast activity, and supporting collagen fiber formation [75, 76].

Numerous studies in functional textile finishing and nanomaterial deposition have been built upon in the creation of bioactive hydrogel-coated fabric dressings for improved pressure ulcer healing. The viability of altering cellulosic substrates to provide long-lasting performance attributes such as hydrophilicity, controlled release behavior, and antibacterial activity was shown by early research into textile auxiliaries and multifunctional finishing systems[77-81]. Specifically, the creation and use of fatty acid/PEG condensates and multipurpose finishing agents offered fundamental knowledge for enhancing the softness, moisture control, and surface reactivity of textiles [79, 80, 82, 83]. By using nano-scale deposition processes, these surface-engineering tactics were further refined, allowing active materials to be incorporated into natural fibers without sacrificing their mechanical integrity [84, 85]. In hydrogel-coated dressings, where close adherence between the hydrogel matrix and textile substrate is essential for preserving structural stability and guaranteeing ideal wound-contact performance, such methods are extremely pertinent.

More recently, the antibacterial properties of medical textiles have been greatly improved by the incorporation of silver nanoparticles (AgNPs) and other metal-based nanostructures into polysaccharide matrices [86-88]. While maintaining the biocompatibility of cellulose-based materials, the impregnation of silver nanoparticles into polysaccharide substrates showed broad-spectrum antibacterial activity [86]. Additionally, controlled-release systems and encapsulation techniques for wound dressings have been investigated to allow for prolonged therapeutic activity, reducing the risk of infection and encouraging tissue regeneration [89-92]. Plant-derived silver nanoparticles can be evenly distributed throughout hydrogel networks when mixed with chemically modified biopolymers like chitosan, alginate, and cellulose derivatives. It creates a multipurpose dressing that can absorb exudate, retain moisture, and provide antimicrobial protection. When taken as a whole, this research offers a strong scientific basis for creating bioactive hydrogel-coated fabric dressings specifically designed to control pressure ulcers. By combining cutting-edge textile chemistry with nanobiotechnology, these dressings can hasten wound healing and lower complications.

In this study, a hydrogel-based wound dressing was developed for pressure ulcer treatment. The hydrogel was formulated using chemically modified chitosan and oxidised alginate, and loaded with plant extracts, biosynthesised silver nanoparticles, and sesame oil. Different formulations were prepared and evaluated to select the most effective one. The final hydrogel was applied to non-woven cotton fabric to produce the dressing. Throughout the study, the prepared materials and the final dressing were characterised and tested to assess their structural, functional, and biological properties relevant to wound healing.

2. Experimental part

2.1. Materials

Chitosan (medium molecular weight, degree of deacetylation around 75–85%) was used as the principal biopolymer and acted as the precursor for the manufacture of O-carboxymethyl chitosan. Sodium alginate (viscosity grade, derived from brown algae) was utilised for the synthesis of oxidised sodium alginate. Both polymers were of analytical quality and acquired from Sigma-Aldrich (Merck Group, USA).

Monochloroacetic acid ($ClCH_2COOH$, ≥99% purity) and sodium hydroxide (NaOH, pellets, ≥98%) were utilised for the carboxymethylation of chitosan. Sodium periodate ($NaIO_4$, ≥99%) was employed as the oxidising agent for alginate modification. Ethylene glycol (≥99%) was utilised as a quenching agent for surplus periodate. The reagents were provided by Merck (Germany).

Isopropanol (≥99.5%), absolute ethanol (≥99.8%), methanol (≥99.8%), and distilled water were employed as solvents for the polymer synthesis, extraction, and purification processes. All solvents were of analytical quality and procured from El-Gomhoria Company for Chemicals, Egypt, unless specified otherwise.

Silver nitrate ($AgNO_3$, ≥99.9% purity), obtained from Sigma-Aldrich (USA), was used as the silver precursor for nanoparticle formation. 0.1 M sodium hydroxide was employed for pH control during the manufacture of nanoparticles.

Phosphate-buffered saline (PBS, pH 7.4) was synthesised in-house utilising analytical-grade sodium chloride, potassium chloride, disodium hydrogen phosphate, and potassium dihydrogen phosphate (Merck, Germany).

Dried aerial components of Hypericum perforatum and dried blossoms of Matricaria chamomilla were procured from a licensed local herbal source (Haraz Herbs, Cairo, Egypt) and verified for authenticity prior to use. Cold-pressed, pharmaceutical-grade sesame oil was acquired from a local pharmaceutical source, Arab Company for Pharmaceuticals, Egypt.

A nonwoven cotton fabric (100% cellulose, medical grade) used as the textile foundation for hydrogel coating and bandage production. The cloth was provided by a local textile producer, Misr Spinning and Weaving Co. in Egypt, and utilised without additional chemical treatment.

Bovine serum albumin (BSA, ≥98% purity) and Bradford reagent, obtained from Sigma-Aldrich (USA), were utilised for protein adsorption investigations. 2,2-Diphenyl-1-picrylhydrazyl (DPPH, ≥95%) was used for the evaluation of antioxidant activity and procured from Sigma-Aldrich (USA).

All microbiological culture medium and reference microbial strains—Staphylococcus aureus (ATCC 29213), Escherichia coli (ATCC 25922), and Candida albicans (ATCC 10231)—were procured from the American Type Culture Collection (ATCC, USA). Media components were acquired from Oxoid (UK).

All compounds were utilised as obtained without further purification unless stated differently.

2.2. Method

2.2.1. Synthesis of O-Carboxymethyl Chitosan (O-CMC)

Carboxymethyl chitosan was synthesised as follows, with slight changes to previously described techniques [93, 94]. Twenty grammes of sodium hydroxide were measured and dissolved in 20 millilitres of distilled water in a beaker. Subsequently, chitosan (20 g) was incrementally introduced to the NaOH solution and meticulously blended using a glass rod until a uniform mixture was achieved. The resultant mixture was subsequently placed in a freezer and allowed to stand for 24 hours to yield alkalised chitosan.

Ten grams of alkalised chitosan was placed into a three-necked round-bottom flask, followed by the addition of 200 mL of isopropanol as a dispersion medium. The suspension was agitated for one hour to achieve uniform dispersion. Monochloroacetic acid (5, 10, 15 g) was thereafter introduced incrementally while maintaining continuous agitation. Following a 30-minute stirring period at ambient temperature, the reaction temperature was raised to 60 °C and sustained for 5 hours.

After the reaction concluded, heating was ceased, and the reaction mixture was let to cool to ambient temperature. The crude carboxymethyl chitosan obtained was collected and subjected to three washes with 100% ethanol to eliminate residual reagents and by-products. The purified product was then diluted in distilled water and dialysed against distilled water for three days. After dialysis, the solution underwent concentration via rotational evaporation and was ultimately dried in an oven to yield carboxymethyl chitosan. The chemical reaction for the manufacture of carboxymethyl chitosan is depicted in Scheme 1.

2.2.2. Synthesis of Oxidised Sodium Alginate (Ox-NaAlg)

Oxidised alginate was synthesised using periodate oxidation in an ethanol-water system to mitigate the severe viscosity constraints linked to alginate oxidation in solely aqueous environments [18]. Sodium alginate was solubilised at a concentration of 20% (w/v) in absolute ethanol with vigorous agitation. Aqueous potassium periodate solution (10, 15, 20% w/v) was subsequently added dropwise to the dispersion at a molar ratio of 1:1 for periodate to alginate monomer units.

The reaction mixture was agitated at ambient temperature for 6 hours in darkness to avert photodegradation of periodate. Upon completion, surplus ethylene glycol was introduced to neutralise unreacted periodate, and agitation was maintained for a further 30 minutes. The oxidised alginate was isolated via precipitation with excess ethanol, subsequently filtered, and thoroughly washed with ethanol and distilled water. The finished product was vacuum-dried at ambient temperature and kept in a desiccator until required. Scheme 2 illustrates the chemical plan for the oxidation of sodium alginate [95].

2.2.3. Preparation of Hypericum Extracts

2.2.3.1. Ethanolic Extract

The dried aerial components of Hypericum were meticulously pulverised, and 10 g of the resultant powder was subjected to extraction using 100 mL of 70% (v/v) aqueous ethanol. The extraction was conducted at 80

°C under reflux for 24 hours. Subsequent to chilling, the extract was subjected to filtration using Whatman No. 1 filter paper to eliminate plant residues. The solvent was eliminated at decreased pressure utilising a vacuum oven at 40 °C. The concentrated extract was then freeze-dried to provide a dry ethanolic extract, which was preserved at −20 °C for future use.

2.2.3.2. Aqueous Extract

A 5% (w/v) aqueous solution of Hypericum powder was formulated with distilled water and subjected to boiling for 15 minutes. The combination was allowed to cool to room temperature and was allowed to stand for 48 hours under ambient conditions. The extract was filtered, and the filtrate was preserved at 4 °C for future studies.

2.2.4. Preparation of Chamomile Extracts

2.2.4.1. Methanolic Extract

Dried chamomile flowers were pulverised into a fine powder. A 5% (w/v) suspension was made by dispersing the powder in methanol and heating the mixture at 65 °C under reflux for 24 hours. After extraction, the mixture underwent filtration to eliminate solid residues, and methanol was entirely evaporated at decreased pressure, utilising a vacuum oven. The methanolic extract was preserved at 4 °C in amber containers until required.

2.2.4.2. Aqueous Extract

Chamomile powder (5%, w/v) was extracted in distilled water by boiling for 15 minutes. The mixture was cooled to ambient temperature and allowed to stand for 48 hours to guarantee full extraction. The extract was filtered and preserved at 4 °C for subsequent use.

2.2.5. Eco-friendly Synthesis of Silver Nanoparticles Utilising Aqueous Plant Extracts

A newly manufactured 1 mM aqueous solution of silver nitrate ($AgNO_3$) was prepared. Equal amounts of $AgNO_3$ solution and aqueous plant extract (Hypericum or chamomile) or ethanolic sesame oil were combined in a 1:1 (v/v) ratio. The reaction mixtures were sustained at 60 °C with continuous magnetic stirring for 4 hours. The pH was modified to 10 with 0.1 M sodium hydroxide to facilitate nanoparticle synthesis.

The diminution of Ag^+ ions was validated by a discernible colour transition from pale yellow to dark brown, signifying the synthesis of silver nanoparticles. The suspensions were cooled to ambient temperature and kept in darkness at 4 °C for subsequent use.

2.2.6. Synthesis of O-CMC/Ox-Alg Hydrogels

Solutions of oxidised sodium alginate (10% w/v) and O-carboxymethyl chitosan (7.5% w/v) were individually produced in phosphate-buffered (PBS, pH 7.4) with continuous stirring at ambient temperature. The two polymer solutions were subsequently combined in volume ratios of 1:4, 2:3, 3:2, and 4:1 (O-CMC: Ox-Alg) to produce various hydrogel compositions.

The mixtures were incubated at 37 °C to facilitate Schiff base formation between the aldehyde groups of oxidised alginate and the amino groups of O-CMC, leading to the creation of a self-crosslinked hydrogel [96] (see Scheme 3).

2.2.7. Fabrication of Hydrogels Infused with Natural Active Compounds

The hydrogel formulation demonstrating superior physicochemical characteristics was chosen for the incorporation of bioactive substances. Ethanolic and methanolic extracts of Hypericum, chamomile, and Sesame oil were included at concentrations of 10%, 15%, and 20% (v/v). Silver nanoparticles produced using aqueous plant extracts were included at concentrations of 5%, 10%, and 15% (v/v). All additives were meticulously blended with the polymer solutions before gelation to guarantee uniform distribution.

2.2.8. Fabrication of Hydrogel-Coated Nonwoven Bandages

The oxidised alginate solution was initially combined with the chosen active ingredient under moderate agitation to achieve uniform dispersion. Subsequently, the O-CMC solution was included, and the mixture was magnetically agitated for approximately one minute. Prior to the onset of full gelation, the reactive hydrogel

solution was uniformly applied to non-woven cotton fabric with a coating process. Gelation occurred in situ at 37 °C, yielding evenly hydrogel-coated cotton bandages appropriate for wound dressing applications.

2.2.9. Application of Hydrogels on Non-Woven Fabric Substrates

Rectangular samples of non-woven fabric (e.g., 5 x 5 cm) were prepared and purified by washing with distilled water, followed by ethanol, to eliminate surface contaminants. The fabric samples were subsequently air-dried at room temperature (RT, 25 ± 2 °C) and preserved in a desiccator before use.

The formulated hydrogel precursor solutions (O-CMC/Ox-NaAlg) with the chosen active agents were applied to the non-woven fabric prior to the onset of gelation. The oxidised alginate solution, including the active ingredient, was initially agitated gently at room temperature to achieve homogeneity. Thereafter, the O-CMC solution was included, and the mixture was agitated for about 1 minute at room temperature under ambient atmosphere conditions to commence crosslinking.

Subsequent to mixing, the viscous hydrogel precursor was evenly applied to the non-woven fabric surface via a dip-coating approach. Each fabric sample was submerged in the hydrogel solution for 2–3 minutes to facilitate adequate infiltration of the polymer matrix into the fibrous structure. Excess hydrogel was eliminated by gently squeezing or draining to guarantee consistent coating thickness.

Gelation occurred in situ on the fabric substrate by incubating the coated samples at 37 °C for 1–2 hours under static circumstances, facilitating full self-crosslinking via Schiff base production. Subsequent to gelation, the hydrogel-coated textiles were air-dried at room temperature under ambient circumstances for 24 hours to eliminate surface moisture.

Thereafter, the samples were further dehydrated in a vacuum oven at 40 °C for 6-8 hours to eliminate residual bound water while preserving the hydrogel structure and bioactive constituents. Subsequent to drying, the hydrogel-coated textiles were positioned in a desiccator with silica gel and maintained in arid conditions at ambient temperature for a minimum of 24 hours before characterisation and subsequent application.

2.3. Analysis and Measurements

2.3.1. Fourier Transform Infrared Spectroscopy (FTIR)

The chemical structure of the synthesised samples was investigated by Fourier-transform infrared (FTIR) spectroscopy using a Bruker Alpha II spectrometer equipped with a Platinum ATR (attenuated total reflectance) accessory, using transmittance modes at a resolution of 2.0 cm−1 in the 4000–500 cm−1 region. Data were acquired and processed using OPUS software.

2.3.2. Scanning Electron Microscopy (SEM)

The surface morphology of the samples was investigated using a JEOL NeoScope™ JCM-7000 benchtop scanning electron microscope. To enhance both image clarity and sample conductivity, the specimens were fixed onto stubs and sputter-coated with a thin layer of gold prior to examination.

2.3.3. Transmission electron microscope (TEM)

Transmission electron microscopy (TEM) was employed to determine the morphology and size of the synthesised nanoparticles. A dilute dispersion of the nanoparticle sample was prepared in an appropriate volatile solvent and ultrasonicated for several minutes to ensure uniform dispersion and to minimise particle agglomeration. A small aliquot of the suspension was then deposited onto a carbon-coated copper grid and allowed to dry at room temperature under ambient conditions.

TEM observations were carried out using a transmission electron microscope operated at an accelerating voltage appropriate for high-resolution imaging. The shape and surface morphology of the nanoparticles were directly examined from the acquired micrographs. Particle size analysis was performed by measuring the diameters of a statistically significant number of nanoparticles from multiple TEM images using image analysis software. The average particle size and size distribution were subsequently calculated and reported to provide a reliable representation of the nanoparticle population.

2.3.4. UV–vis spectroscopy

UV–visible spectral analysis of the AgNPs was performed using a Cary 100 UV-Vis-NIR instrument (Agilent Technologies), scanning wavelengths from 300 to 800 nm at 2 nm resolution.

2.3.5. Determination of the degree of substitution (DS)

The degree of substitution (DS) of carboxymethyl chitosan (CMCS) was determined using a titrimetric method, following established procedures. A precisely weighed 0.10 g CMCS sample was dissolved in 20 mL of distilled water. The resulting solution was acidified with standardised 0.10 M hydrochloric acid until the pH was reduced to below 2.0. The acidified solution was then titrated with 0.050 M aqueous sodium hydroxide (NaOH). During titration, the solution was continuously stirred, and pH values were recorded simultaneously until the pH reached 11.5. The titration curve obtained from this process was used to identify the two inflection points required for subsequent calculations.

The degree of substitution was calculated using the following equation:

$$DS = \frac{161\,A}{M-58A}$$

where A represents the amount of NaOH consumed between the two inflection points and is given by

$$A = V_{NaOH} \times C_{NaOH}.$$

Here, V_{NaOH} is the volume of NaOH solution consumed, and C_{NaOH} is the molarity of the NaOH solution (0.050 mol·L−1. M denotes the mass of the CMCS sample (in grams). The molecular weights of the carboxymethyl substituent and the glucosamine unit were taken as 58 and 161 g·mol−1, respectively.

The degree of substitution of the synthesized o-carboxymethyl chitosan has been calculated to be 0.6

2.3.6. Measuring Carboxyl content.

The combustion method was used to determine the percent of carboxyl groups in carboxymethyl-chitosan. The ash method determines carboxyl group content (–COOH) by converting carboxyl groups into their metal salts (usually calcium or sodium), followed by ashing at high temperature. The residual ash weight corresponds to the amount of metal bound to carboxyl groups, which is then used to calculate the carboxyl content. [97]

The carboxyl content is calculated from the ash mass using stoichiometric relationships.

$$\text{Carboxyl content (mmol/g)} = [W_{ash} \times 1000] / [M_{metal\ oxide} \times W_{sample}]$$

Where: W_{ash} = mass of ash (g), W_{sample} = dry sample mass (g), $M_{metal\ oxide}$ = molar mass of ash compound (e.g., Na_2CO_3 = 106 g/mol),

The carboxyl content of the synthesized carboxymethyl ghitosan was found to be 6 mmol/g.

2.3.7. Solubility tests

The water solubility of the materials was evaluated at room temperature using visual observation. Initially, 20 mg of the sample was dispersed in 100 mL of distilled water and thoroughly mixed using a vortex mixer to ensure complete dissolution. Once a clear and homogeneous solution was obtained, additional portions of 10 mg of the material were incrementally introduced into the solution with continuous mixing. This process was repeated until visible precipitation occurred.

The solubility limit was defined as the total mass of material added to the solution immediately prior to the onset of precipitation. This value was taken as a measure of the maximum amount of material that could be dissolved in water under the experimental conditions.

2.3.8. Determination the Oxidation Degree

The degree of oxidation of sodium algenate was determined using the hydroxylamine hydrochloride titration method, following the procedure reported by Zhao et al. [98]. The degree of oxidation is defined as the number of oxidised units per 100 repeating **units** of the polymer. In this method, oxidised sodium alginate was reacted with an excess amount of hydroxylamine hydrochloride. The reaction between aldehyde groups and hydroxylamine hydrochloride generates hydrochloric acid, the quantity of which is directly proportional to the aldehyde content present in the oxidised polymer.

The hydrochloric acid produced was subsequently titrated with a standardised sodium hydroxide (NaOH) solution, and the volume of NaOH consumed at the equivalence point was recorded. The degree of oxidation was calculated according to the following Equation.

$$\text{Degree of oxidation (\%)} = \frac{V_{NaOH} \times C_{NaOH} \times M_{repeat}}{n_{max} \times n} \times 100$$

where V_{NaOH} represents the volume of NaOH consumed, C_{NaOH} is the concentration of the NaOH solution (0.1 M), $n_{C=O}$ denotes the maximum possible number of aldehyde groups, m is the dry mass of oxidised sodium

algenate (0.1 g), and M is the molecular weight of the sodium algenate repeating unit (approximately **198.11 g/mol**). For sodium algenate, up to eight aldehyde groups can be generated per repeating unit as a result of oxidative cleavage of the C–C bonds between adjacent hydroxyl-bearing carbon atoms (–CHOH). [99]

2.3.9. Gelation Time

The gelation time of self-crosslinked oxidised alginate/carboxymethyl chitosan was determined using the tube inversion technique[100]. In this method, hydrogel solutions with specified compositions were prepared in 100 mL glass vials and incubated at 37°C. The gelation process was monitored by inverting the vials at 37°C, and the gelation time was recorded when the hydrogel solution ceased to flow, indicating the formation of a gel.

2.3.10. Swelling Test

The swelling ratio was determined using a method previously reported in the literature [96, 101]. The crosslinked hydrogels were soaked in a PBS solution and incubated at 37°C for 24 hours to allow them to swell completely. After incubating and equilibrating, the hydrogels were removed, and their swollen weights (Ws) were recorded. The samples were then dried under vacuum, and the dry weights (Wd) were recorded. The swelling ratio was determined using the following formula:

$$\text{swelling ratio} = \frac{Ws - Wd}{Wd} \text{x } 100$$

2.3.11. Protein Adsorption Test

The protein adsorption by the hydrogel membranes was assessed using Bovine Serum Albumin (BSA) as the protein model. The experimental procedure was adapted from previously established methodologies in literature [102, 103]. A 5% (w/v) solution of BSA was prepared in phosphate-buffered saline (PBS, pH 7). For the adsorption test, 10 mL of BSA solution was added to the hydrogel samples. The samples were incubated in an orbital shaker at 200 rpm and 37°C for 24 hours. Upon completion of the incubation, the samples were removed from the protein solution, and aliquots of the remaining solution were collected. Both the initial and equilibrium protein concentrations were determined spectrophotometrically using the Bradford reagent. A 100 µL aliquot of both the initial and remaining protein solutions was mixed with 1 mL of Bradford reagent and 2 mL of distilled water. The concentration of proteins was quantified by measuring the absorbance at 595 nm using a Cary 100 UV-Vis-NIR spectrophotometer (Agilent Technologies). The amount of protein adsorbed by the hydrogel membranes was calculated using the following equation:

$$q = \frac{(C_0 - C_e) \times V}{m}$$

where q (mg/g) represents the adsorption capacity; C_0 and C_e (mg/L) are the initial and equilibrium protein concentrations in the solution, respectively; V (L) is the volume of the solution; and m (g) is the mass of the adsorbent.

2.3.12. Antioxidant Efficiency

The antioxidant ability of the prepared hydrogels was evaluated by assessing the free radical scavenging activity of DPPH, following the method previously described by Jeong, J.-P et al. (2025) [104]. A total of 50 mg of prepared hydrogels was added to 5 mL of a 0.1 mM DPPH solution (EtOH: DW, 1:1) and incubated at 30°C for 30 minutes in the dark. After incubation, the absorbance of the DPPH solution was measured at 517 nm using UV-vis spectrophotometry. The DPPH radical scavenging activity was calculated using the following equation:

$$\text{DPPH radical scavenging activity\%} = \left(\frac{A_0 - A_s}{A_0}\right) \text{x}100$$

Where A_0 represents the absorbance of the DPPH solution in EtOH: DW (1:1), and A_s is the absorbance of the solution containing the hydrogel.

2.3.13. Nitrogen content

The nitrogen content of samples was quantitatively determined using the Kjeldahl method, as described in Vogel's Textbook of Quantitative Chemical Analysis [105-108].

2.3.14. Converting Nitrogen Loss (%) → Moles of Imine Bonds Formed

Nitrogen in the hydrogel originates exclusively from O-CMC amino groups**. Each** imine (–C=N–) bond consumes one primary amine**, i.e.,** 1 mol N → 1 mol imine bond**.** Nitrogen is quantified as **mass % (w/w)** via Kjeldahl analysis.

Step 1: Nitrogen loss calculation

For a given hydrogel:

$$\Delta N(\%) = N_{O\text{-}CMC} - N_{hydrogel}$$

Where: $N_{O\text{-}CMC}$= (native O-CMC) and $N_{hydrogel}$ = measured nitrogen %

Step 2: Convert nitrogen loss to moles of nitrogen

For 1 g of dry hydrogel:

$$nN_{consumed} = \frac{\Delta N}{100} \times \frac{1}{14.011}$$

Where 14.011 $g \cdot mol^{-1}$ is the atomic mass of nitrogen.

Imine crosslink density ≈ 0.51 mmol g^{-1}

Normalisation of Imine Density per Repeating Unit

To normalise the imine (Schiff-base) density to the polymer structure, the molar density of imine bonds ($mol \cdot g^{-1}$) was converted to the **number of imine bonds per alginate repeating unit**, using the molecular weight of the sodium alginate repeat unit:

$$M_{Alg}\ repeat \approx 198\ g\backslash cdotpmol$$

The normalised imine content was calculated as:

$$\text{Imine bonds per repeating unit} = n_{imine} \times Mr_{epeat}$$

2.3.15. Release Study

The release behavior of the encapsulated oils or extraction from the prepared hydrogel matrix or treated gauze fabric was evaluated under controlled conditions. Briefly, 1 g of the encapsulated oils or extraction formulation was immersed in 100 mL of phosphate-buffered saline (PBS, pH 7.5) and incubated at 37 °C on a simple shaker (Multi Mix MTR-22) operating under a programmed shaking and rotation mode. The release study was conducted over a period of 6 h, during which 5 mL aliquots were withdrawn at predetermined time intervals (15, 30, 60, 120, 180, 240, 300, and 360 min). The concentration of the released oil or extraction was quantified using a UV–Vis spectrophotometer (Carry 100). After each sampling, the withdrawn volume was immediately replaced with an equal volume of fresh PBS to maintain a constant total volume. The cumulative oil or extraction release was expressed as a percentage according to the relationship Oil or extraction.

$$\text{Release } (\%) = (Ct/C0) \times 100$$

where C0 represents the initial amount of oil or extracted loaded, and Ct denotes the amount of oil or extraction released at time t. All experiments were performed in triplicate to ensure reproducibility.

2.3.16. Antibacterial test

The antibacterial efficacy was quantitatively assessed against *Staphylococcus aureus* (ATCC 29213; Gram-positive), *Escherichia coli* (ATCC 25922; Gram-negative), and *Candida albicans* (ATCC 10231; fungal strain) using the AATCC 100-2004 standard test method for antimicrobial activity evaluation [109]. This method involves the preparation of a homogeneous microbial suspension in a liquid growth medium, which is subsequently brought into contact with the test material under sterile conditions. The samples containing the thickening agent were incubated with the microbial inoculum in sealed containers at 37 °C for 24 h. Following incubation, the samples were agitated for 1 min to detach viable microorganisms, and the surviving microbial population was quantified. Antimicrobial activity was expressed as the percentage reduction (%R) in microbial count relative to the initial inoculum.

3. Result and Discussion

3.1. Characterisation of O- carboxymethyl chitosan

The effective synthesis of O-carboxymethyl chitosan (O-CMC) was validated using reaction route analysis (Scheme 1), FTIR spectroscopy (Figure 1), and quantitative assessment of the degree of substitution (DS) (Table 1). Scheme 1 demonstrates that the carboxymethylation process occurs through nucleophilic substitution between the alkoxide groups formed on chitosan in strong alkaline conditions and monochloroacetic acid, preferentially targeting the hydroxyl groups over the amino groups. The selectivity of this reaction aligns with the synthetic process, wherein chitosan was initially alkalised with strong NaOH and then distributed in isopropanol, a heterogeneous medium recognised for inhibiting excessive N-substitution while facilitating O-carboxymethylation.

Chitosan contains several reactive functional groups, including hydroxyl groups at the C3 and C6 positions, a primary amine group at C2, as well as acetylated amino residues and glycosidic linkages. These groups differ in their reactivity during carboxymethylation, where the C6 hydroxyl is typically the most susceptible to substitution, followed by the amino group at C2 and the C3 hydroxyl [93]. In O-carboxymethylation, the reaction primarily targets the hydroxyl group at the C6 position, replacing it with a carboxymethyl moiety. This modification pathway is depicted in Scheme 1, which outlines the substitution mechanism on the Chitosan backbone.

The FTIR spectra (Figure 1) unequivocally demonstrate successful chemical change. Native chitosan (Cs) displays distinct broad absorption bands near 3400 cm^{-1}, attributed to overlapping O–H and N–H stretching vibrations, alongside peaks at roughly 1655 cm^{-1} (amide I) and 1590 cm^{-1} (–NH_2 bending). [64] After carboxymethylation, the FTIR spectrum of CMC displays a more intense and broadened absorption band around 3400 cm^{-1}, indicative of enhanced O–H and N–H stretching [110]. In addition, the O-CMC spectra reveal the appearance of additional absorption bands at about 1605–1620 cm^{-1} and 1415–1430 cm^{-1}, corresponding to the asymmetric and symmetric stretching vibrations of carboxylate groups (–COO^-), respectively. The emergence and gradual enhancement of these bands, together with a relative reduction in the intensity of the –NH_2 bending vibration, validate the successful incorporation of carboxymethyl groups into the chitosan backbone. Furthermore, increased absorption in the 1050–1150 cm^{-1} range, linked to C–O–C and C–O stretching vibrations, further substantiates substitution at the hydroxyl sites, aligning with O-selective carboxymethylation rather than broad amine alteration. [111]

The quantitative study of substitution degree (Table 1) indicates a distinct correlation between the degree of substitution (DS) and the quantity of monochloroacetic acid utilised in the synthesis. Augmenting the MCA content from 5 to 15 g led to a systematic increase in DS from 0.28 ± 0.03 to 0.96 ± 0.05, illustrating effective regulation of functionalisation via reaction stoichiometry. The O-CMC10 sample (DS = 0.58 ± 0.04) exemplifies an ideal equilibrium between improved water solubility and the retention of free amino groups, essential for biological activity and electrostatic interactions. Conversely, the elevated degree of substitution (DS) noted for O-CMC15, although enhancing solubility, may partially hinder the accessibility of protonated –NH_2 groups, potentially diminishing intrinsic antibacterial efficacy. A significant enhancement in the carboxyl content (–COOH) was observed following the etherification process, attributed to the successful introduction of –CH_2–COOH groups into the chitosan backbone. The –COOH concentration increased from 0.3 mmol/kg in the native chitosan to 0.6 mmol/kg in the synthesised carboxymethyl chitosan (CMC), confirming the effectiveness of the modification. The integrated spectroscopic and compositional studies definitively validate the successful and adjustable synthesis of O-carboxymethyl chitosan, affirming the efficacy of the employed alkalisation–heterogeneous carboxymethylation approach.

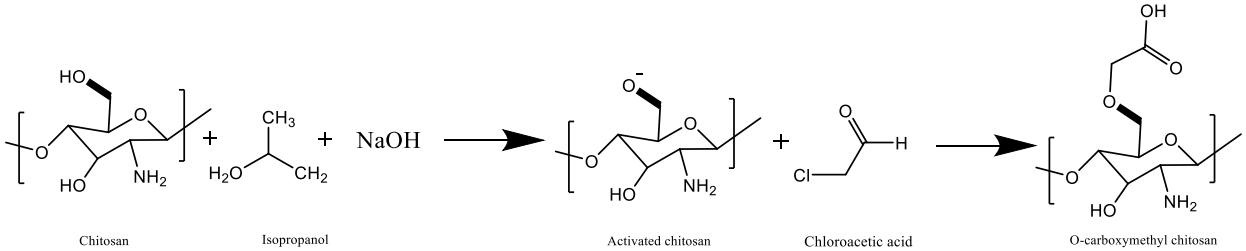

Scheme 1: Schematic illustration of the carboxymethylation of chitosan

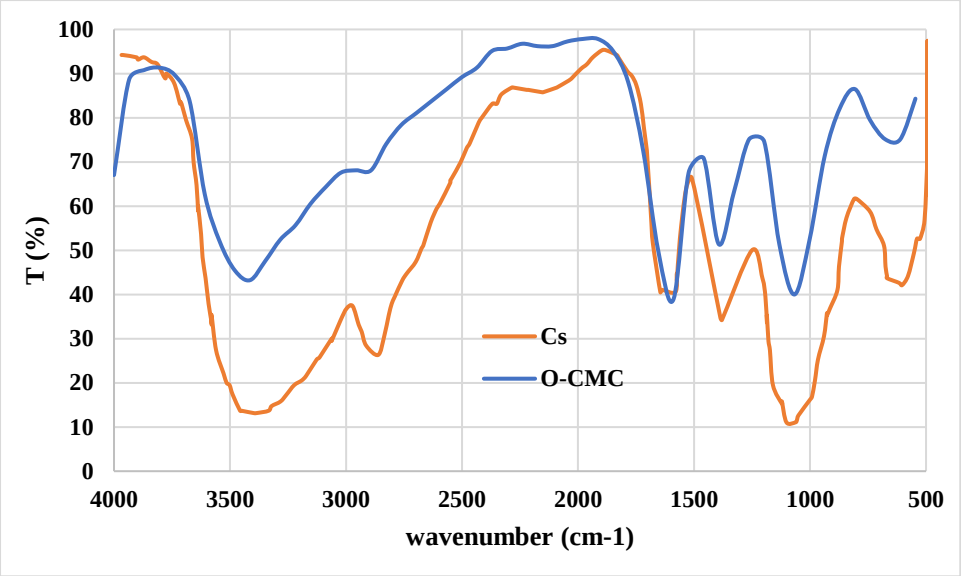

Figure 1: FTIR spectra for the chitosan and carboxymethyl chitosan.

Table 1: Degree of Substitution (DS) of O-Carboxymethyl Chitosan

Sample code	MCA amount (g)	DS (–)	Carboxyl content (mmol/kg)	Interpretation
Native chitosan (Cs)	**0**	0.00	0.3	Insoluble, limited reactivity
O-CMC5	**5**	0.28 ± 0.03	0.42	Partial solubility, high NH_2 retention
O-CMC10	**10**	**0.58 ± 0.04**	0.54	Optimal solubility–reactivity balance
O-CMC15	**15**	0.96 ± 0.05	0.66	High solubility, reduced antibacterial NH_2

A degree of substitution (DS) between about 0.55 and 0.65 is considered ideal for O-carboxymethyl chitosan used in wound dressing and hydrogel applications. Multiple investigations indicate that DS values ranging from 0.4 to 0.7 achieve an optimal equilibrium between water solubility and functional group accessibility, essential for medicinal efficacy. At this amount of substitution, enough carboxymethyl groups are included to interrupt inter- and intramolecular hydrogen bonding within the chitosan backbone, therefore markedly improving water solubility in physiological settings. A significant proportion of primary amino ($–NH_2$) groups stays unaltered, maintaining their crucial functions in antibacterial activity, bioadhesion, and electrostatic interactions. This DS family is especially compatible with Schiff-base hydrogel systems, where free $–NH_2$ groups are necessary to interact with the aldehyde functions of oxidised polysaccharides (e.g., oxidised alginate) to establish dynamic imine connections. Prior studies on self-crosslinked chitosan–aldehyde hydrogels indicate that degree of substitution (DS) values between 0.5 and 0.6 facilitate effective gel formation, manageable gelation kinetics, and advantageous mechanical and biological characteristics [62, 94, 95]. Consequently, the detected degree of substitution within this range is both chemically plausible and functionally beneficial for wound healing and injectable hydrogel systems.

3.2. Characterisation of Oxidised Alginate

The successful oxidation of sodium alginate was validated via reaction pathway analysis (Scheme 2), FTIR spectroscopy (Figure 2), and quantitative assessment of the oxidation degree (Table 2). Scheme 2 illustrates that periodate oxidation selectively cleaves the C2–C3 vicinal diol bonds of the alginate backbone, producing reactive dialdehyde functionalities while maintaining the polymeric structure. In the first step, sodium metaperiodate reacts with these hydroxyl groups to form a temporary cyclic structure. This intermediate then breaks down, leading to the cleavage of the bond between C2 and C3. As a result, two aldehyde groups are introduced into each oxidised monomer unit [112]. The utilisation of an ethanol–water reaction medium was essential in alleviating excessive chain scission and viscosity-related constraints commonly found in entirely aqueous systems, thus facilitating controlled oxidation under mild circumstances. The oxidised alginate, now containing dialdehyde groups, becomes more reactive and can be further cross-linked through Schiff base reactions or other covalent interactions. It enhances its potential use in forming hydrogels for biomedical applications.

FTIR spectra furnish substantial evidence for this structural alteration. Native alginate displays distinct broad absorption bands at around 3400 cm^{-1} linked to O–H stretching [113], as well as significant bands near 1600 and 1410 cm^{-1} related to the asymmetric and symmetric stretching vibrations of carboxylate groups ($–COO^-$) [96, 112]. Oxidised alginate (Ox-Alg) exhibits significant spectral alterations upon oxidation, characterised by a decrease in the intensity of hydroxyl-related bands and the appearance or amplification of absorption in the 1720–1740 cm^{-1} range, corresponding to the stretching vibration of newly formed aldehyde (–CHO) groups [65-68, 96, 112, 114]. Moreover, modifications in the fingerprint region (1000–1200 cm^{-1}) indicate the disruption of the pyranose ring structure due to C–C bond cleavage, thereby further validating successful periodate oxidation. In the native alginate spectrum, peaks at 815 and 1078 cm^{-1} — characteristic of symmetrical C–O–C stretching — were present, but these peaks were significantly diminished in the oxidised form, confirming structural alterations [99].

Quantitative examination (Table 2) reveals a distinct correlation between the degree of oxidation and the quantity of sodium periodate utilised, with values rising from 11.2 ± 1% to 44.1 ± 3% as the $NaIO_4$ concentration escalated. This incremental rise correlates with the creation of around 0.23 to 0.86 aldehyde groups per alginate repeating unit, signifying efficient and adjustable aldehyde production. Moderate oxidation levels (≈25–45%) are particularly beneficial for biomedical applications, since they offer adequate aldehyde functionality for Schiff-base crosslinking with amine-containing polymers, such as carboxymethyl chitosan, while preventing severe backbone breakdown. The results together affirm that the implemented ethanol-assisted periodate oxidation method facilitates precise regulation of alginate functionalisation, yielding oxidised alginate with a defined aldehyde content appropriate for dynamic hydrogel production and wound dressing applications.

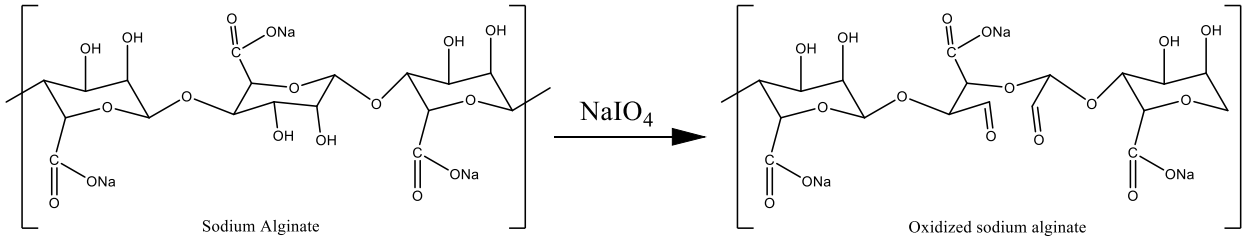

Scheme 2: Schematic illustration of the oxidation of sodium alginate

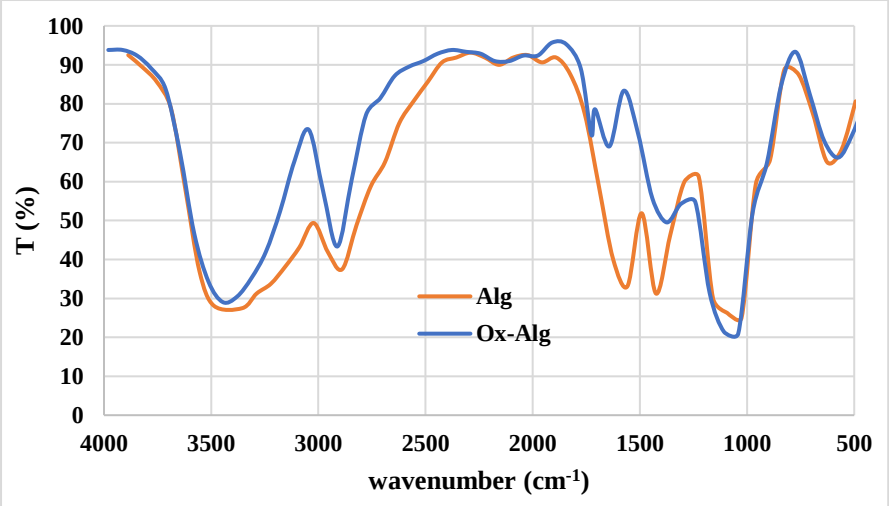

Figure 2: FTIR of sodium alginate and oxidised sodium alginate.

Table 2: Oxidation Degree of Sodium Alginate

Sample code	$NaIO_4$ amount (g)	Oxidation Degree (%)	Aldehyde Groups per Unit
Native Alginate (Alg)	**0**	0	**0**
Ox-Alg10	**5**	11.2 ± 1	0.23
Ox-Alg15	**10**	**26.4 ± 2**	**0.54**
Ox-Alg20	**15**	44.1 ± 3	0.86

The degree of oxidation is crucial in determining the structural integrity and mechanical performance of alginate-based hydrogels. Reports indicate that oxidation levels of around 30–35% cause substantial deterioration of the alginate backbone due to widespread cleavage of the C2–C3 bonds, leading to diminished molecular weight, impaired chain entanglement, and inadequate mechanical stability. Excessive oxidation compromises the natural polysaccharide structure, resulting in brittle or weak hydrogels with diminished load-bearing capacity and inadequate handling properties. A moderate oxidation level of 20–30% is universally recognised as suitable for injectable and textile-based hydrogel systems. This range produces adequate aldehyde groups for effective Schiff-base crosslinking with amine-containing polymers, while preserving the polymer's mechanical integrity, elasticity, and cohesive strength. This equilibrium facilitates manageable gelation kinetics, injectability, and conformability, which are critical attributes for wound dressings and biomedical textile applications. Thus, sustaining the oxidation level within this moderate range is essential for producing functional hydrogels that exhibit both chemical reactivity and mechanical strength.

3.3. Characterisation of Silver nanoparticles

The generation and structural properties of silver nanoparticles (AgNPs) synthesised using Hypericin and chamomile extracts were validated using UV–Vis spectroscopy (Figure 3) and transmission electron microscopy (TEM) (Figure 4). The UV–Vis spectra display clear surface plasmon resonance (SPR) bands, indicative of AgNP production due to the collective oscillation of conduction electrons on the nanoparticle surface. Silver nanoparticles synthesised with chamomile extract have a distinct surface plasmon resonance peak centred at 420–440 nm, whilst those made with hypericin extract demonstrate a marginally larger and red-shifted surface plasmon resonance band, reaching towards approximately 450 nm. The changes in SPR location and bandwidth signify variances in particle size distribution, morphology, and surface chemistry, attributable to the unique phytochemical compositions of the plant extracts serving as reducing and stabilising agents. The lack of comparable SPR peaks in the spectra of the pure extracts verifies that the detected plasmonic characteristics stem only from nanoparticle production, not from inherent chromophores. The slight broadening of the SPR bands indicates a polydisperse nanoparticle population, frequently observed in biosynthesized AgNP systems due to the intricate variety of biomolecules involved in reduction and capping. [86, 115, 116]

TEM micrographs (Figure 4a,b) offer direct visual validation of nanoparticle production and further clarify the impact of biological reducing agents on nanoparticle morphology. Silver nanoparticles synthesised using chamomile extract generally display quasi-spherical morphology with significant aggregation, likely due to partial surface coverage by flavonoids and phenolic chemicals that provide insufficient steric stabilisation. Conversely, AgNPs synthesised with hypericin extract exhibit a more uniform size distribution and decreased agglomeration, indicating enhanced capping efficiency linked to hypericin's polyaromatic structure and its numerous functional groups that can coordinate silver ions. The nanoscale dimensions identified in both systems align with the SPR characteristics noted in UV–Vis spectra. The synthesis conditions—high temperature (60 °C), alkaline pH (≈10), and extended reaction duration—are essential for enhancing Ag^{+} reduction and facilitating nanoparticle nucleation, while the plant-derived biomolecules concurrently function as stabilising agents, inhibiting excessive particle growth. The results collectively affirm that the implemented eco-friendly synthesis method facilitates the effective creation of AgNPs with adjustable optical and morphological characteristics, principally influenced by the type of plant extract utilised as the bioreductant and capping agent.

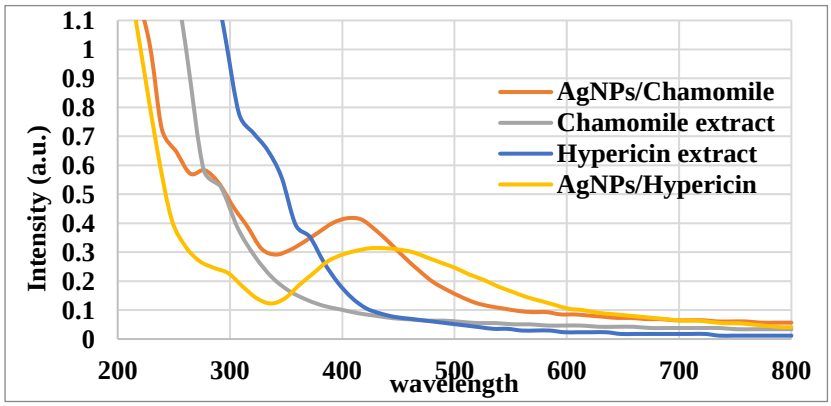

Figure 3: UV–Vis spectra of silver nanoparticles synthesised using Hypericin and Chamomile extracts

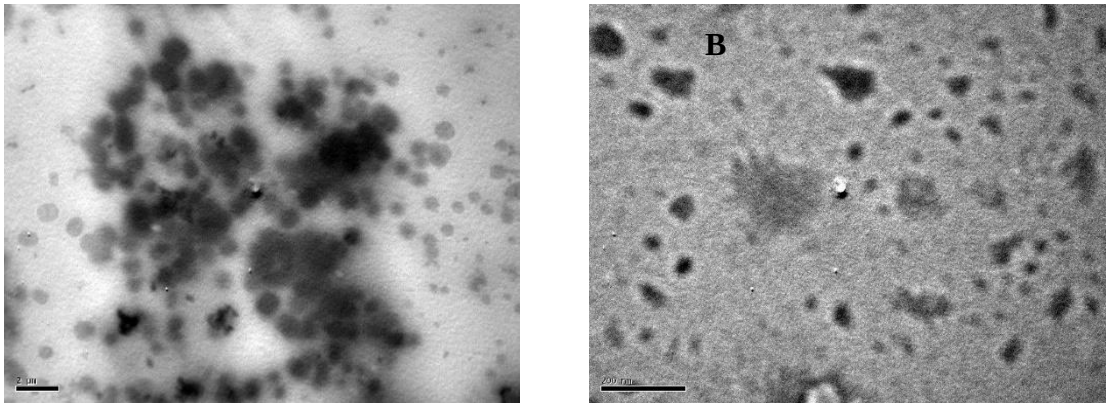

Figure 4: TEM images for the synthesis of silver nanoparticles
a) using chamomile extract, and b) hypericin extract

3.4. Characterisation of O-CMC/Na-Alg Hydrogel

The synthesis of self-crosslinked O-CMC/Ox-NaAlg hydrogels was validated using reaction mechanism analysis (Scheme 3) and FTIR spectroscopy of polymer mixtures generated at various compositional ratios (Figure 5). Scheme 3 demonstrates that hydrogel formation is facilitated by Schiff-base reactions between aldehyde groups produced from oxidised sodium alginate and the free amino groups of O-carboxymethyl chitosan, leading to dynamic imine (–C=N–) linkages that serve as covalent crosslinks within the polymer network.

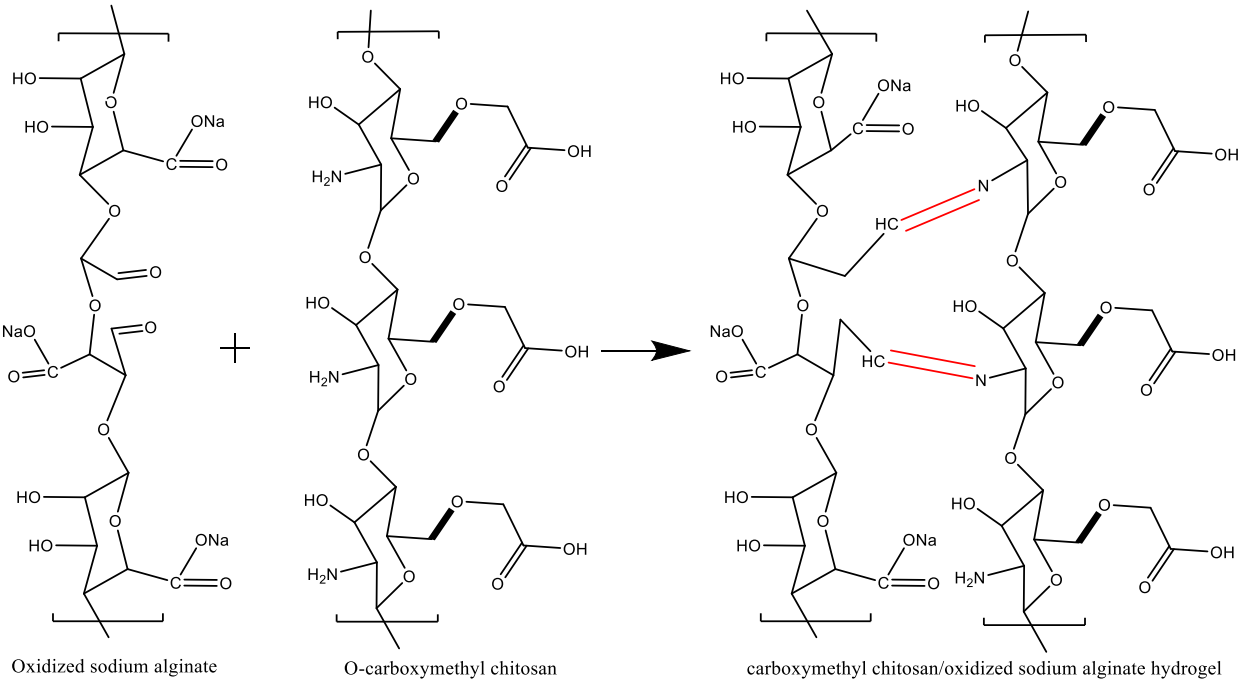

Scheme 3: reaction mechanism between Ox-Alg and O-CMC

3.4.1. FTIR

FTIR spectra offer unequivocal molecular-level evidence of these interactions. In comparison to the spectra of pristine O-CMC and Ox-NaAlg, the hydrogel spectra demonstrate significant attenuation of the aldehyde-related band typically found around 1720–1740 cm^{-1} in oxidised alginate, along with alterations in the amide/amine region near 1580–1650 cm^{-1}, signifying the consumption of –CHO and $–NH_2$ groups during imine bond formation [96, 117]. Moreover, the appearance and expansion of absorption bands in the 1620–1640 cm^{-1} range indicate the creation of Schiff-base (C=N) connections, hence affirming successful chemical crosslinking as opposed to mere physical blending. The extensive O–H/N–H stretching band in the range of 3200–3500 cm^{-1}

becomes increasingly prominent and experiences a modest shift with varying O-CMC: Ox-NaAlg ratios, indicating increased hydrogen bonding and network densification within the hydrogel matrix. Fluctuations in spectrum intensity at various ratios demonstrate that crosslinking density is significantly influenced by composition, with intermediate ratios (e.g., 2:3 and 3:2) showing more marked spectral alterations, indicating a more equitable distribution of reactive aldehyde and amine groups. These observations correspond with the synthesis conditions, wherein incubation at 37 °C in PBS (pH 7.4) facilitates effective Schiff-base production under physiologically relevant conditions. The FTIR results clearly indicate the effective synthesis of chemically crosslinked O-CMC/Ox-Alg hydrogels, with adjustable network topologies determined by polymer ratios, confirming their appropriateness for biomedical hydrogel and wound-dressing applications.

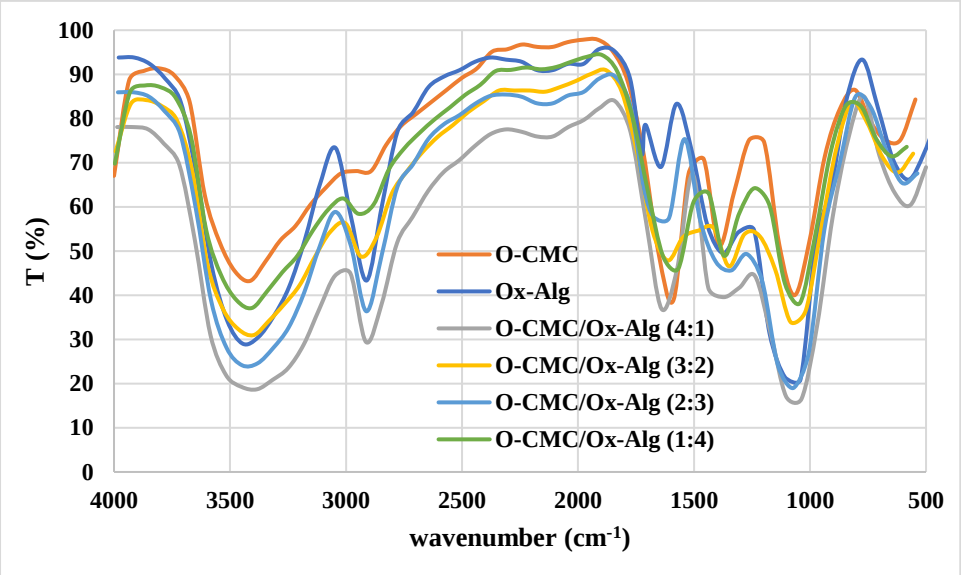

Figure 5: FTIR spectra of O-CMC: Ox-Alg mixtures at various ratios

3.4.2. Relationships Among Hydrogel Composition, Structure, and Properties

Table 3 summarises the compositional dependence of nitrogen concentration, gelation time, and swelling behaviour of the synthesised O-CMC/Ox-Alg hydrogels, offering useful insights into the development of network structure and crosslinking efficiency. As anticipated, native O-CMC demonstrated the largest nitrogen content (1.821%), indicative of its richness in primary amino groups, whereas oxidised alginate displayed minimal nitrogen content (0.091%), corroborating the absence of nitrogen-containing functions in its polysaccharide backbone. Following hydrogel formation, a gradual reduction in nitrogen content was noted with an increase in Ox-Alg fraction, signifying the systematic utilisation of free amino groups via Schiff-base interactions with aldehyde functionalities. This trend offers indirect yet persuasive evidence of effective covalent crosslinking, since heightened aldehyde availability facilitates imine bond formation and diminishes the quantity of detectable free $–NH_2$ groups within the hydrogel matrix.

The gelation period demonstrated a significant influence on the polymer ratio, underscoring the necessity of stoichiometric equilibrium among reactive functional groups. The O-CMC/Ox-Alg (3:2) formulation exhibited the quickest gelation time (12 minutes), closely succeeded by the (2:3) formulation (15 minutes), indicating that near-equimolar availability of amine and aldehyde groups promotes swift network development. Conversely, the (4:1) formulation necessitated a considerably extended gelation period (80 min), due to inadequate aldehyde concentration to swiftly crosslink the many amine groups. Excessive oxidised alginate in the (1:4) formulation led to extended gelation (45 min), probably due to the dilution of amine sites and diminished chain entanglement efficiency. These findings emphasise that optimal gelation kinetics occur at intermediate compositions, where functional group complementarity and molecular mobility are maximised.

The swelling behaviour further confirms the impact of crosslink density and network architecture on hydrogel performance. Hydrogels with elevated O-CMC content demonstrated enhanced swelling ratios, with the (4:1) formulation exhibiting the highest swelling (18.08%), indicative of reduced crosslink density and increased availability of hydrophilic groups for water absorption. In contrast, an increase in Ox-Alg concentration resulted in a significant decrease in swelling ratio, attaining a minimum of 9.81% for the (1:4) formulation. This decrease is ascribed to elevated crosslink density resulting from enhanced aldehyde–amine interactions, which

constrain polymer chain mobility and impede water passage into the network. Intermediate formulations (3:2 and 2:3) exhibited balanced swelling behaviour (≈16–17%), reflecting well-structured networks that integrate adequate mechanical strength with regulated hydration—attributes greatly sought after for wound dressing and injectable hydrogel applications.

The results in Table 3 indicate that the characteristics of hydrogels can be precisely adjusted by manipulating the composition of O-CMC and Ox-Alg. Formulations with intermediate ratios attain an ideal equilibrium between swift gelation, moderate swelling, and efficient crosslinking, rendering them especially appropriate for biomedical applications where injectability, structural integrity, and moisture regulation are essential.

3.4.3. Quantitative Relationship Between Nitrogen Utilisation and Schiff-Base Crosslink Density

The study of nitrogen content offers quantitative insight into the degree of Schiff-base formation and, therefore, the crosslink density within the O-CMC/Ox-Alg hydrogel network. Table 3 indicates that native O-CMC contains a nitrogen concentration of 1.821%, reflecting its elevated density of free primary amino groups. A systematic decrease in nitrogen content is noted with an increasing proportion of Ox-Alg upon hydrogel formation, indicating the gradual consumption of $–NH_2$ groups during the formation of imine (–C=N–) bonds with aldehyde groups on oxidised alginate. The nitrogen content diminishes from 1.532% in the O-CMC/Ox-Alg (4:1) hydrogel to 0.625% in the (1:4) formulation, indicating an overall nitrogen reduction of roughly 66% compared to pristine O-CMC. This substantial depletion validates thorough covalent crosslinking instead of simple physical blending. Intermediate compositions, specifically (3:2) and (2:3), exhibit nitrogen concentrations of 1.111% and 0.935%, respectively, reflecting a regulated utilisation of 39–49% of available amino groups. These formulations correspond to the minimal gelation durations and equilibrated swelling ratios, signifying that an ideal Schiff-base density is attained when aldehyde and amine functionalities exist in almost stoichiometric ratios. Excessive nitrogen retention at elevated O-CMC levels causes reduced crosslink density and extended gelation, whereas excessive nitrogen depletion at high Ox-Alg concentrations results in too dense networks with limited swelling. Nitrogen consumption acts as a dependable quantitative indicator of Schiff-base crosslink density, establishing a direct correlation between molecular-scale chemical reactions and macroscopic hydrogel characteristics, including gelation kinetics and hydration behaviour.

3.4.4. Crosslink Density of Imine (Schiff-Base) in the Synthesized Hydrogels

The molar density of imine (Schiff-base) bonds quantitatively assesses the effective crosslink density in the O-CMC/Ox-Alg hydrogel network and elucidates structure–property correlations. Pristine O-CMC demonstrates a low imine density (2.06×10^{-4} mol·g^{-1}), indicating the lack of aldehyde groups and verifying the absence of covalent crosslinking without oxidised alginate. The gradual integration of Ox-Alg significantly enhances imine bond density, indicating effective aldehyde–amine coupling during hydrogel synthesis. The O-CMC/Ox-Alg (4:1) formulation has a modest imine density (5.07×10^{-4} mol·g^{-1}), suggesting restricted crosslink production owing to inadequate aldehyde availability in relation to amine groups. Elevating the Ox-Alg content to intermediate ratios markedly improves crosslink density, with the (3:2) and (2:3) formulations demonstrating imine densities of 6.32×10^{-4} and 8.54×10^{-4} mol·g^{-1}, respectively. These compositions exhibit a near-stoichiometric equilibrium between aldehyde and amine functionalities, facilitating optimal Schiff-base production and enhanced network connection. The increased crosslink density is directly associated with the quickest gelation periods and balanced swelling ratios seen in experiments, signifying swift network formation and regulated water absorption. Conversely, augmenting Ox-Alg concentration beyond this ideal range is anticipated to hinder effective crosslinking due to the dilution of amine sites and heightened chain scission, ultimately undermining network homogeneity and mechanical performance. The results collectively indicate that intermediate O-CMC/Ox-Alg compositions achieve the highest effective imine crosslink density, which supports their enhanced gelation kinetics, dimensional stability, and mechanical integrity, rendering them especially appropriate for biomedical hydrogel applications.

The normalisation of imine bond density to the alginate repeating unit offers a molecular-level comprehension of crosslink production within the O-CMC/Ox-Alg hydrogel network. Pristine O-CMC demonstrates a minimal imine density of roughly 0.04 imine bonds per repeating unit, resulting from the absence of aldehyde functionalities and confirming the lack of intrinsic covalent crosslinking. The insertion of oxidised alginate consistently raises the imine concentration with the amount of Ox-Alg, indicating improved aldehyde–amine interaction. The O-CMC/Ox-Alg (4:1) formulation demonstrates roughly 0.10 imine bonds per repeating unit, signifying restricted crosslinking due to an insufficiency of aldehydes in relation to the available amine groups. Conversely, intermediate compositions exhibit significantly elevated crosslink densities, with the (3:2) and (2:3) formulations attaining roughly 0.13 and 0.17 imine bonds per repeating unit, respectively. These figures suggest that about one Schiff-base linkage is established for every 6–8 alginate repeat units, signifying a highly efficient

and uniform crosslinked network. Significantly, these intermediate formulations correspond with the minimal gelation periods, optimal swelling ratios, and enhanced mechanical integrity seen experimentally, validating that near-stoichiometric availability of aldehyde and amine groups maximises effective crosslink density. Significant divergence from this equilibrium—whether by aldehyde restriction or amine dilution—diminishes the quantity of imine bonds generated per repeating unit, resulting in delayed gelation and impaired network efficacy. The normalised imine density serves as a reliable quantitative measure connecting molecular-scale chemistry to macroscopic hydrogel characteristics, confirming the superiority of intermediate O-CMC/Ox-Alg compositions for biomedical hydrogel applications.

Table 3: Characteristics of synthesised hydrogel

	N (%)	n_{imine} (mol.g^{-1})	Imine bonds per repeating unit	Gelation time (min)	Swelling ratio (%)
O-CMC	1.821		0.041	--	--
O-CMC /Ox-Alg (4:1)	1.532	2.06×10^{-4}	0.1	80	18.08
O-CMC/Ox-Alg (3:2)	1.111	$\mathbf{5.07\times10^{-4}}$	0.13	12	17.49
O-CMC/Ox-Alg (2:3)	0.935	6.32×10^{-4}	0.17	15	16.52
O-CMC/ Ox-Alg (1:4)	0.625	8.54×10^{-4}	-	45	9.81
Ox-Alg	0.091		0	--	--

3.5. Characterisation of impregnated AgNPs and bioactive compounds in a hydrogel network

3.5.1. Behaviour of Hydrogels Infused with Silver Nanoparticles and Bioactive Substances

The physicochemical and biological properties of the O-CMC/Ox-Alg hydrogel were significantly affected by the incorporation of plant-derived bioactive chemicals and silver nanoparticles, as detailed in Table 4. In comparison to the unaltered hydrogel, all modified systems demonstrated notable alterations in gelation kinetics, swelling characteristics, nitrogen content, antioxidant efficacy, and protein adsorption, illustrating the intricate interactions among Schiff-base crosslinking, secondary interactions, and filler integration within the polymeric matrix.

The findings in Table 4 indicate that the incorporation of bioactive chemicals and AgNPs facilitates precise modulation of hydrogel gelation, swelling, chemical properties, and biological efficacy. Extract-loaded systems promote quick gelation and enhanced antioxidant and protein adsorption capacities, whereas the inclusion of AgNP results in prolonged gelation periods and regulated swelling, potentially benefiting sustained antibacterial applications. The findings underscore the adaptability of the O-CMC/Ox-Alg hydrogel platform and its appropriateness for multifunctional biomedical and wound-healing applications via strategic compositional design.

Table 4: characteristics of the impregnated AgNPs and bioactive compounds in a hydrogel network

	Bioactive Conc. (%)	Gelation time(min)	Swelling ratio (%)	N (%)	Antioxidant Activity (%)	Protein adsorption (mg/g)
Gel only		12	17.49	1.111	18.54	0.115
Ethanolic Hypericin	10	15	4.23	0.691	33.55	0.175
	15	11	5.43	1.021	41.59	0.169
	20	7	5.53	1.351	54.57	0.185
Methanolic Chamomile	10	16	4.08	1.274	18.69	0.225
	15	13	8.38	1.884	25.45	0.229
	20	8	9.56	2.494	37.91	0.175
Sesam oil	5	15	13.22	0.317	7.95	0.376
	10	22	9.01	0.468	11.86	0.416
	15	34	4.68	0.619	16.29	0.361
AgNPs-Aqueous Hypericin	5	30	9.44	0.237	14.11	0.086
	10	50	16.81	0.351	19.14	0.078
	15	90	40.31	0.465	28.67	0.056
AgNPs-Aqueous Chamomile	5	48	17.61	0.252	4.42	0.369
	10	80	26.33	0.373	15.32	0.335
	15	98	50.21	0.494	26.42	0.295
AgNPs-Sesame oil	5	9	3.66	0.190	4.82	0.169
	10	15	2.12	0.281	7.39	0.164
	15	47	14.79	0.372	22.10	0.135

3.5.2. Nitrogen content

The study of nitrogen concentration offers direct information on network chemistry and the availability of functional groups. Compared to the unmodified hydrogel (1.111% N), extract-loaded systems had markedly elevated nitrogen levels, suggesting reduced utilisation of amino groups during Schiff-base formation as a result of competitive interactions with bioactive chemicals. The effect was particularly significant for chamomile-loaded hydrogels, aligning with their greater extract polarity and enhanced affinity for amino functions. AgNP-impregnated hydrogels exhibited relatively diminished nitrogen levels, especially at reduced nanoparticle concentrations, indicating increased amine utilisation and/or nanoparticle interaction with nitrogenous groups, so concealing them from elemental analysis.

Figure 6 depicts the fluctuation in nitrogen content (N%), which acts as a quantitative indicator for free and used amino groups, in both the pristine hydrogel and hydrogel networks infused with bioactive chemicals and silver nanoparticles. The O-CMC/Ox-Alg hydrogel displays a moderate nitrogen concentration (~1.11%), indicating partial utilisation of primary amine groups via Schiff-base formation with the aldehyde groups of oxidised alginate. Following impregnation with ethanolic hypericin, a significant and concentration-dependent elevation in nitrogen content is noted, peaking at around 2.49% at the highest loading level. This trend signifies the effective integration of nitrogen-rich phytochemical components and/or enhanced hydrogen-bonding and coordination interactions between hypericin functional groups and the polymer matrix, thereby augmenting the total nitrogen contribution without completely compromising the covalent imine crosslinks.

A comparable yet more prominent impact is observed in methanolic chamomile-loaded hydrogels, where nitrogen content significantly increases with higher loading, attaining around 2.49%. This improvement is due to the increased polarity of methanolic extracts and their greater abundance of amino- and heterocycle-containing bioactives, which are more effectively maintained within the hydrogel matrix. Conversely, sesame oil–infused hydrogels exhibit significantly reduced nitrogen levels (≈0.31–0.62%), aligning with the nitrogen-deficient, hydrophobic characteristics of the oil. The diluting impact from oil inclusion and the diminished availability of hydrophilic domains likely inhibit both nitrogen contribution and effective Schiff-base density.

Hydrogels infused with AgNPs synthesised from aqueous plant extracts demonstrate a unique nitrogen evolution profile. Despite a progressive increase in nitrogen content with AgNP concentration, the absolute values remain inferior to those of extract-only systems. This behaviour indicates partial masking or consumption of amine groups resulting from coordination with AgNP surfaces, along with steric restriction caused by nanoparticle inclusion, which restricts additional imine bond formation. The diminished nitrogen levels noted at elevated AgNP concentrations correspond with extended gelation durations and decreased swelling documented in other studies, affirming that excessive nanoparticle integration undermines network flexibility and the availability of reactive sites.

Figure 6 indicates that the chemical composition and concentration of impregnated agents significantly influence nitrogen content. Extract-loaded systems augment nitrogen content via additive functional groups and secondary interactions, while AgNP-loaded systems exhibit competitive amine consumption and coordination effects. These results offer robust quantitative evidence connecting nitrogen balance to Schiff-base density, gelation kinetics, and hydrogel functionality, highlighting the significance of regulated impregnation to maintain network integrity while enhancing bioactivity.

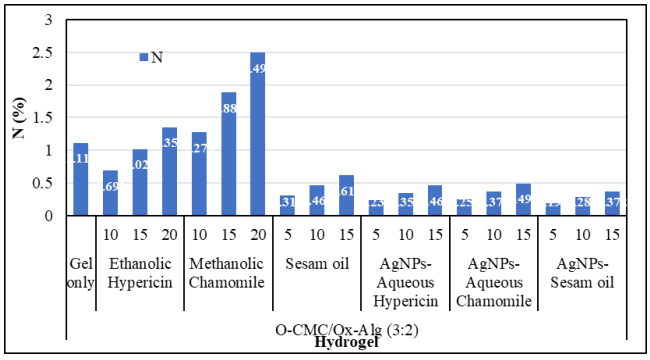

Figure 6: Nitrogen content of hydrogels

3.5.3. Gelation time

The kind and concentration of the impregnated agent significantly influenced the gelation period. Hydrogels infused with ethanolic hypericin and methanolic chamomile extracts exhibited gradually diminished gelation times as extract concentration increased, achieving a minimum of 7–8 minutes at the highest concentrations. This characteristic can be ascribed to the existence of polyphenolic and aromatic groups that facilitate enhanced

hydrogen bonding and π–π interactions, therefore expediting network development and stabilising imine cross-links. Conversely, hydrogels containing AgNPs—especially those synthesised with aqueous plant extracts—demonstrated significantly extended gelation periods, reaching up to 90–98 minutes at elevated nanoparticle concentrations. This slowdown is ascribed to steric hindrance and the partial shielding of reactive amino and aldehyde groups by nanoparticles, which impedes Schiff-base formation and chain diffusion during gelation.

Figure 7 illustrates the gelation time profiles of the unmodified O-CMC/Ox-Alg hydrogel and the associated networks infused with bioactive extracts, oils, and silver nanoparticles, highlighting significant variations in gelation kinetics influenced by network chemistry and additive interactions. The hydrogel demonstrates a brief gelation period (about 12 minutes), aligning with the effective Schiff-base synthesis between the aldehyde groups of oxidised alginate and the main amine groups of O-CMC at physiological temperature. The fast gelation indicates a balanced ratio of reactive functional groups and unfettered molecular mobility, facilitating quick imine bond formation and network percolation.

The use of ethanolic hypericin and methanolic chamomile extracts significantly decreases gelation time at higher concentrations, with the lowest values around 7–8 minutes. The acceleration is due to the presence of polyphenolic and carbonyl-containing chemicals in the extracts, which enhance hydrogen bonding and secondary interactions, thereby pre-organizing polymer chains and expediting crosslink production. Furthermore, the moderately polar characteristics of these extracts improve miscibility with the hydrogel matrix, preserving chain flexibility while augmenting the local reaction likelihood between aldehyde and amine groups.

Conversely, sesame oil-infused hydrogels have a non-linear pattern, with gelation time significantly rising at elevated oil concentrations. The hydrophobic characteristics of the oil create phase heterogeneity and diminish reactive functional groups, therefore obstructing polymer–polymer interaction and decelerating Schiff-base kinetics. This impact is more pronounced at high oil loadings, when gelation periods exceed 30–40 minutes, signifying postponed network development and diminished crosslinking effectiveness.

A significantly distinct behaviour is seen for AgNP-loaded hydrogels. Systems including AgNPs synthesised with aqueous hypericin or chamomile extracts exhibit a significant, concentration-dependent prolongation of gelation time, attaining around 90–98 minutes at the maximum nanoparticle concentrations. This significant slowdown is ascribed to the robust interaction between silver nanoparticles and the amino groups of O-CMC, which competitively depletes or sterically obstructs the amine functions necessary for Schiff-base formation. Moreover, the inflexible nanoparticle domains impede chain mobility and diffusion, thereby prolonging the formation of the gel network. AgNPs synthesised using sesame oil have significantly shorter gelation durations, indicating diminished nanoparticle–polymer interactions and less disruption of amine availability.

Figure 7 unequivocally illustrates that the chemical composition and concentration of the impregnated substances significantly influence gelation time. Polar plant extracts can expedite gelation by improving intermolecular contacts, whereas the inclusion of hydrophobic oils and nanoparticles—especially at elevated concentrations—considerably hinders network development. These findings underscore the imperative to equilibrate bioactive loading with crosslinking chemistry to produce hydrogels with adjustable gelation kinetics appropriate for injectable, in situ forming, or textile-based wound dressing applications.

In conclusion, the incorporation of natural extracts, silver nanoparticles synthesised via plant-water extracts, and sesame oil had a notable impact on the gelation time of the hydrogel system. The addition of alcoholic extracts of Hypericin and chamomile significantly reduced the gelation time, depending on the added concentration. As the proportion of these extracts increased, the gelation process accelerated, reaching complete gel formation within approximately 7 minutes. Conversely, the addition of silver nanoparticles synthesised using aqueous extracts of Hypericum and chamomile markedly prolonged the gelation time, extending it to approximately 98 minutes.

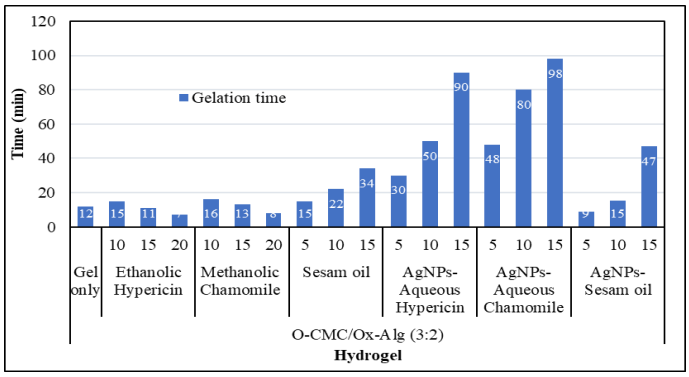

Figure 7: Gelation time of hydrogels

3.5.4. Swelling ratio

The swelling behaviour further indicated these structural alterations. Extract-impregnated hydrogels often show moderate decreases in swelling ratio compared to the gel-only system, aligning with heightened effective crosslink density and diminished free volume. In contrast, AgNP-loaded hydrogels exhibited significant swelling at elevated nanoparticle concentrations, especially in aqueous systems driven by hypericin and chamomile. This abnormal swelling signifies network weakening due to nanoparticle aggregation and the establishment of a heterogeneous architecture, resulting in extra voids and disrupting uniform crosslinking. Sesame oil-based systems exhibited a clear trend: swelling initially rose with oil content due to plasticization effects, but decreased at higher concentrations as hydrophobic domains restricted water absorption.

Figure 8 depicts the swelling characteristics of the unmodified O-CMC/Ox-Alg hydrogel and the associated networks infused with bioactive extracts, oils, and silver nanoparticles, emphasising the significant influence of network structure and additive composition on water absorption. The hydrogel demonstrates a modest swelling ratio (~17.5%), indicative of a balanced crosslink density resulting from effective Schiff-base formation between the aldehyde groups of oxidised alginate and the amino groups of O-CMC. This intermediate swelling is indicative of well-structured covalent networks that maintain enough hydrophilicity while preventing excessive chain relaxation. [96, 118]

Hydrogels infused with ethanolic hypericin exhibit a significant decrease in swelling ratio at low concentrations, succeeded by a steady rise at elevated levels. This behaviour indicates that the integration of the original extract enhances intermolecular interactions—such as hydrogen bonding and π–π stacking—resulting in network densification and limited water transport. At increased hypericin levels, the extract introduces additional polar functional groups that improve hydrophilicity, partially mitigating crosslink tightening and augmenting water absorption. A similar tendency is noted for methanolic chamomile-loaded hydrogels, however, with elevated swelling values overall, due to the more hydrophilic characteristics of chamomile bioactives and their capacity to disturb dense polymer arrangement. [119]

Conversely, hydrogels infused with sesame oil demonstrate consistently reduced swelling ratios, especially at elevated oil concentrations. The hydrophobic oil domains decrease the effective water-accessible volume and restrict polymer–water interactions, leading to reduced swelling. This behaviour validates partial phase separation and underscores the function of hydrophobic additives in inhibiting hydrogel hydration, although the presence of hydrophilic polysaccharide backbones.

A drastically altered swelling profile is seen for AgNP-loaded hydrogels. Systems comprising AgNPs synthesised with aqueous hypericin or chamomile extracts exhibit a significant enhancement in swelling ratio, with values of 40–50% at elevated nanoparticle concentrations. This improvement results from the breakdown of covalent crosslinks caused by amine coordination with AgNP surfaces, leading to a reduction in effective Schiff-base density and an increase in network porosity. The existence of stiff nanoparticle domains generates microvoids and heterogeneous areas that promote water infiltration and retention. In contrast, AgNPs synthesised in sesame oil demonstrate somewhat diminished swelling, aligning with decreased nanoparticle dispersion and weaker hydrophilic interactions.

Figure 8 illustrates that a nuanced equilibrium of crosslink density, hydrophilicity, and structural heterogeneity regulates the swelling behaviour. Moderate extract loading maintains network integrity while facilitating regulated hydration, whereas excessive nanoparticle incorporation results in over-swelling owing to crosslink breakage. The findings are crucial for optimising hydrogel performance in wound dressings and biomedical textiles, where regulated swelling is vital for preserving moisture balance, mechanical stability, and continuous bioactive release.

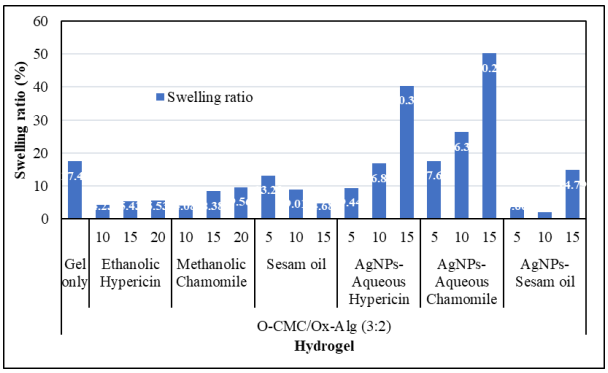

Figure 8: swelling ratio of hydrogels

3.5.5. Protein adsorption study

It is widely recognised that wound dressings with low protein adsorption capacity offer multiple therapeutic benefits. By limiting protein accumulation at the dressing interface, they help reduce local inflammation, preserve a moist wound environment, and promote more effective interaction between the wound bed and the dressing. These characteristics collectively enhance tissue regeneration, minimise the risk of bacterial colonisation and secondary infections, and improve patient comfort by reducing dressing adherence and pain upon removal. Additionally, such properties often reduce the frequency of dressing changes, thereby supporting a more stable healing process[120].

To evaluate the protein adsorption behavior of the developed biohybrid hydrogel membranes, a protocol adapted from previously reported methodologies [102, 103] was employed. Bovine serum albumin (BSA) was selected as the model protein due to its prevalence in wound exudates and its wide application in adsorption studies [121].

The behaviour of protein adsorption demonstrated further linkages between structure and function. Extract-impregnated hydrogels, specifically those loaded with chamomile, demonstrated superior protein adsorption capabilities (up to 0.229 mg g^{-1}), indicating enhanced surface functionality, polarity, and accessibility of hydrogen-bonding sites. Conversely, AgNP-loaded hydrogels exhibited significantly decreased protein adsorption, particularly at elevated nanoparticle concentrations, presumably owing to pore obstruction, surface passivation by nanoparticles, and electrostatic repulsion phenomena. Hydrogels derived from sesame oil exhibited elevated protein adsorption, correlating with enhanced surface roughness and protein affinity mediated by hydrophobic interactions.

Figure 9 illustrates the protein adsorption capabilities of both pure and modified O-CMC/Ox-Alg hydrogels, offering significant insight into the relationship among network chemistry, surface functionality, and bioactive loading. The hydrogel demonstrates a modest protein adsorption capacity (~0.115 $mg \cdot g^{-1}$), typical of moderately crosslinked polysaccharide networks with restricted exposed binding sites. The regulated consumption of amino groups via Schiff-base synthesis diminishes the presence of positively charged sites, therefore limiting nonspecific protein-surface interactions.

The introduction of ethanolic hypericin results in a gradual rise in protein adsorption, exceeding 0.40 $mg \cdot g^{-1}$ at moderate loading levels. This improvement is due to the incorporation of aromatic and phenolic groups, which facilitate protein adsorption via π–π interactions, hydrogen bonding, and van der Waals forces. The adsorption peaks at moderate hypericin levels and diminishes marginally at elevated concentrations, indicating potential pore obstruction or steric hindrance that restricts protein transport into the hydrogel matrix. A comparable, however, more significant tendency is noted for methanolic chamomile-loaded hydrogels, which exhibit the greatest adsorption capabilities among the extract-based systems. The prevalence of hydroxyl- and carboxyl-rich flavonoids in chamomile increases hydrophilicity and offers many binding motifs, hence strengthening protein–polymer interactions.

Conversely, hydrogels infused with sesame oil have markedly reduced protein adsorption capabilities, especially at elevated oil concentrations. The hydrophobic domains created by the oil diminish surface wettability and obscure polar functional groups, thereby inhibiting protein interaction. This behaviour aligns with the reduced swelling ratios and suggests restricted protein access to the hydrogel interior.

AgNP-impregnated hydrogels exhibit a unique adsorption characteristic. Systems comprising AgNPs synthesised with aqueous plant extracts exhibit significant protein adsorption at low nanoparticle concentrations, which thereafter decreases progressively with increasing AgNP concentration. This decrease is ascribed to the interaction of proteins with amine groups at the nanoparticle surface, together with steric hindrance effects resulting from nanoparticle aggregation inside the hydrogel matrix. Furthermore, AgNPs can confer localised stiffness, restricting chain mobility and diminishing the effective surface area accessible for protein adsorption. AgNPs synthesised using sesame oil demonstrate reduced adsorption, indicating decreased nanoparticle dispersion and poorer interactions with protein molecules.

Figure 9 illustrates that a nuanced interplay of hydrophilicity, surface charge, porosity, and additive chemistry regulates protein adsorption. Hydrogels infused with extracts, especially chamomile, exhibit increased protein affinity, beneficial for wound healing applications, as protein adsorption facilitates cell adhesion and tissue regeneration. On the contrary, the regulated decrease of protein adsorption in AgNP-rich systems may be advantageous for mitigating biofouling and inflammatory reactions. The results underscore the adaptability of the hydrogel substrate for customised biological interactions by deliberate modification of network composition and functional additives.

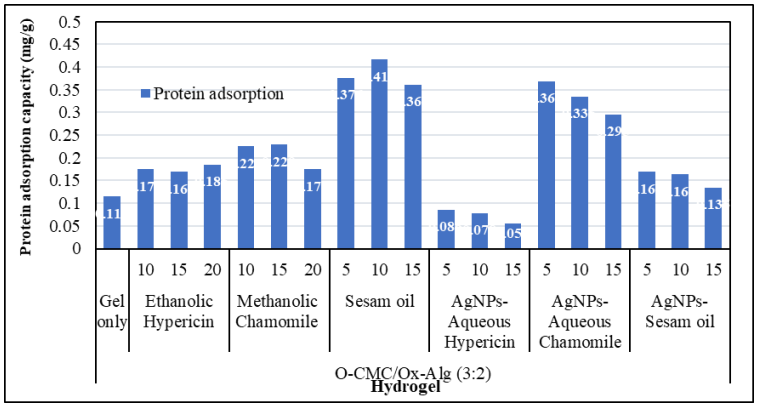

Figure 9: Protein adsorption capacity of the hydrogel formulations

3.5.6. Antioxidant Activity of Hydrogels

Delayed wound healing is strongly linked to oxidative stress caused by the excessive production of reactive oxygen species (ROS). At low levels, ROS support normal healing by promoting cell movement and the formation of new blood vessels. However, high levels of ROS can harm cells, interfere with cell signaling, extend inflammation, and reduce blood vessel formation. In pressure ulcer wounds, large amounts of ROS—produced by inflammatory cells through NADPH oxidase—can worsen tissue damage. Antioxidants help reduce this damage by neutralising ROS, which supports proper wound healing and tissue recovery [122, 123]. Therefore, modulating the inflammatory response is essential to minimising oxidative damage and subsequent scar formation [101, 124]**.**

Hydrogels are widely recognised as ideal wound dressings due to their biocompatibility, permeability, and ability to maintain a moist environment conducive to healing. Moreover, specific hydrogel formulations can exhibit intrinsic antioxidant properties, further enhancing their therapeutic effect by reducing oxidative stress.

The antioxidant capacity of the hydrogel formulations was determined using the DPPH radical scavenging method. As presented in Figure 10, all samples exhibited significant activity in reducing DPPH radicals, confirming their efficiency as free radical scavengers. The findings indicate that the concentration of the incorporated bioactive compounds directly influences the antioxidant activity of the hydrogels. Specifically, higher concentrations of the extracts resulted in hydrogels with significantly enhanced antioxidant potential.

Functionally, impregnation significantly improved antioxidant activity compared to the gel-only approach (18.54%). Ethanolic hypericin-loaded hydrogels exhibited superior antioxidant efficiency, achieving up to 54.57%, due to hypericin's significant radical-scavenging ability and its efficient retention inside the hydrogel matrix. Methanolic chamomile systems demonstrated concentration-dependent antioxidant improvement, albeit to a lesser degree, indicating variations in phenolic content and extract efficacy. Hydrogels containing AgNP exhibited moderate antioxidant activity, which intensified with increased nanoparticle concentration, owing to the synergistic interactions between metallic silver and plant-derived capping agents; nonetheless, these values were inferior to those of extract-only systems due to the restricted accessibility of active phytochemicals when adhered to nanoparticle surfaces.

Figure 10 depicts the DPPH radical scavenging activity of both pure and functionalised O-CMC/Ox-Alg hydrogels, clearly indicating the significant impact of integrated bioactive chemicals and silver nanoparticles on antioxidant efficacy. The hydrogel has a moderate scavenging activity (~18.5%), attributable to the inherent antioxidant properties of chitosan-derived amino groups and residual hydroxyl functionalities. The partial utilisation of $–NH_2$ groups during Schiff-base crosslinking restricts the intrinsic radical-quenching ability of the native network.

The inclusion of ethanolic hypericin results in a significant, concentration-dependent increase in antioxidant activity, surpassing 50%. This notable rise correlates with the elevated presence of phenolic hydroxyl groups and conjugated aromatic systems in hypericin, which serve as potent hydrogen and electron donors, effectively stabilising DPPH radicals. The gradual rise during loading signifies effective trapping and preservation of hypericin inside the hydrogel matrix, without significant deterioration of its antioxidant properties. Likewise, methanolic chamomile-loaded hydrogels have improved radical scavenging action, albeit to a lesser degree than hypericin-based systems. This behaviour indicates the presence of flavonoids and phenolic acids in chamomile extracts, which enhance antioxidant activity via hydrogen atom transfer and metal chelation pathways.

Conversely, hydrogels infused with sesame oil demonstrate relatively less antioxidant activity, especially at reduced oil concentrations. The restricted radical scavenging seen aligns with the decreased quantity of phenolic antioxidants in the oil phase and the hydrophobic characteristics of the oil, which impede effective interaction between antioxidant moieties and DPPH radicals in the test medium. Nonetheless, a minor rise at elevated loadings indicates a partial contribution from lipid-soluble antioxidant constituents, including sesamol and sesamin.

Hydrogels, including AgNPs synthesised with aqueous plant extracts, exhibit a moderate antioxidant activity. At minimal nanoparticle concentrations, antioxidant activity is constrained, presumably due to the partial occlusion of phenolic groups by coordination with the silver surface and reduced mobility within the matrix. Increased AgNP concentrations result in a significant boost in scavenging activity, likely due to synergistic interactions between residual phytochemicals capping the nanoparticles and the augmented surface area accessible for radical interactions. Nonetheless, these values are inferior to those of extract-only systems, suggesting that nanoparticle production partially diminishes free antioxidant efficacy.

Figure 10 illustrates that antioxidant activity is predominantly influenced by the characteristics and accessibility of phenolic bioactives rather than just by the polymeric matrix. Hydrogels infused with extracts, especially those containing hypericin, have enhanced radical scavenging capabilities, positioning them as viable options for modulating oxidative stress in wound healing applications. The flexibility to modulate antioxidant potential via regulated impregnation further underscores the adaptability of the O-CMC/Ox-Alg hydrogel substrate for multifunctional biomedical dressings. [125].

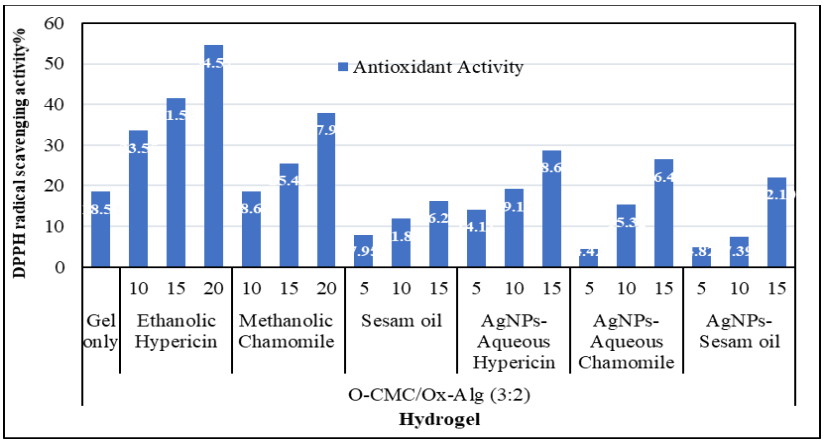

Figure 10: DPPH radical scavenging activity of the hydrogel formulations

3.6. Characterization of Non-woven bandage loaded with hydrogels

3.6.1. Physicochemical and biofunctional characteristics

Table 5 encapsulates the physicochemical and biofunctional attributes of untreated and hydrogel-treated nonwoven textiles, distinctly illustrating the transformational impact of hydrogel impregnation on textile efficacy. The untreated cloth displays little nitrogen concentration, antioxidant activity, and protein adsorption, affirming its inert chemical properties and absence of intrinsic bioactivity. Conversely, all textiles treated with hydrogel exhibit significant increases in nitrogen content, indicating the effective deposition and preservation of nitrogen-rich polysaccharide networks and bioactive constituents within the fibrous matrix.

The fabric infused with the neat O-CMC/Ox-Alg hydrogel exhibits a moderate nitrogen content of 1.11%, aligning with the presence of chitosan-derived amino groups that have been largely used in Schiff-base crosslinking. This treatment provides significant antioxidant activity (18.54%) and quantifiable protein adsorption (0.115 $mg \cdot g^{-1}$), demonstrating that the hydrogel coating successfully transforms the inert textile into a biointeractive surface. The addition of ethanolic hypericin significantly improves textile functioning, resulting in the greatest antioxidant activity (54.57%) of all samples. This significant impact is ascribed to the elevated phenolic content and conjugated aromatic structures of hypericin, which preserve their radical scavenging ability post-immobilization inside the hydrogel matrix. The simultaneous rise in nitrogen content indicates effective retention of both polymeric and extract-derived functional groups on the fabric surface.

Fabrics treated with methanolic chamomile have the greatest nitrogen content (2.49%), indicating the prevalence of nitrogen- and oxygen-rich phytochemicals in the extract and their effective incorporation into the hydrogel matrix. The antioxidant activity of chamomile-treated textiles, while inferior to that of hypericin-based systems, is nonetheless significant at 37.91%, attributable to the presence of flavonoids and phenolic acids.

Significantly, chamomile-treated textiles exhibit balanced protein adsorption, suggesting advantageous surface chemistry for biological interactions.

Fabrics infused with sesame oil have relatively diminished nitrogen concentration and antioxidant activity, aligning with the oil's hydrophobic and nitrogen-deficient characteristics. These samples demonstrate the greatest protein adsorption (0.361 $mg \cdot g^{-1}$), indicating that hydrophobic features and decreased surface charge facilitate nonspecific protein binding. This behaviour may benefit specific applications, but it also suggests a possible risk of excessive biofouling if not meticulously managed.

Fabrics infused with AgNP-laden hydrogels display unique properties. Notwithstanding reduced nitrogen levels—due to amine interaction with AgNP surfaces—their antioxidant properties persist at modest levels, indicating the influence of phytochemical capping agents on the nanoparticles. Protein adsorption is significantly diminished in AgNP-hypericin systems, suggesting an anti-fouling effect possibly due to silver-induced protein denaturation or electrostatic repulsion. Conversely, AgNP-chamomile systems exhibit notably increased protein adsorption, underscoring the preeminent role of extract chemistry in modulating surface contacts, beyond the impacts of nanoparticles.

Table 5 illustrates that hydrogel impregnation enables the exact manipulation of textile bioactivity via the regulated integration of polymers, plant extracts, and nanoparticles. The findings underscore the capacity to independently adjust nitrogen content, antioxidant capacity, and protein adsorption, offering a flexible foundation for sophisticated wound dressings that necessitate concurrent balanced antioxidant protection, regulated protein interaction, and antimicrobial efficacy.

Table 5: Characteristics of untreated and treated nonwoven fabric with different hydrogel formulations

Fabric	N (%)	Antioxidant Activity (%)	Protein adsorption (mg/g)
Untreated Fabric	0.01	0	0
Gel only	1.111 ± 0.015	18.54 ± 1.15	0.115 ± 0.012
Ethanolic Hypericin	1.351 ± 0.018	54.57 ± 1.85	0.185 ± 0.019
Methanolic Chamomile	2.494 ± 0.027	37.91 ± 1.75	0.175 ± 0.018
Sesam oil	0.619 ± 0.021	16.29 ± 3.61	0.361 ± 0.036
AgNPs-Aqueous Hypericin	0.465 ± 0.018	28.67 ± 0.56	0.056 ± 0.006
AgNPs-Aqueous Chamomile	0.494 ± 0.021	26.42 ± 2.95	0.295 ± 0.03
AgNPs-Sesame oil	0.372 ± 0.013	22.1 ± 1.35	0.135 ± 0.013

3.6.2. Antimicrobial activity

Table 6 illustrates the quantitative antimicrobial efficacy of untreated and hydrogel-treated nonwoven fabrics against Staphylococcus aureus, Escherichia coli, and Candida albicans, effectively showcasing the synergistic interactions of polymeric hydrogels, plant-derived bioactives, and silver nanoparticles. The untreated cloth shows no antibacterial properties, demonstrating its inert nature and validating that the observed decreases in microbes result only from the applied hydrogel compositions.

The fabric infused with the neat O-CMC/Ox-Alg hydrogel exhibits moderate antimicrobial efficiency, demonstrating more effectiveness against S. aureus (42%) than E. coli (31%) and C. albicans (18%). This pattern aligns with the inherent antibacterial characteristics of chitosan, which largely function through electrostatic interactions between protonated amino groups and negatively charged microbial cell membranes. The diminished efficacy against Gram-negative bacteria and fungi is due to the protective outer membrane of E. coli and the resilient cell wall architecture of C. albicans, which restrict polymer–cell interactions.

The inclusion of ethanolic hypericin and methanolic chamomile extracts markedly improves antibacterial efficacy against all evaluated pathogens. Hypericin-impregnated textiles demonstrate greater reductions than chamomile-treated samples, achieving up to 71% efficacy against S. aureus. This enhanced action is ascribed to hypericin's potent photodynamic and membrane-disruptive characteristics, together with its capacity to produce reactive oxygen species that undermine microbial viability. Fabrics treated with chamomile have significant antibacterial properties due to the presence of flavonoids, terpenoids, and phenolic acids, which damage microbial membranes and interfere with metabolic processes. Fabrics treated with sesame oil have modest antibacterial activity, attributable to lipid-soluble antimicrobial compounds such as sesamol; nonetheless, their effectiveness is inferior to that of polar plant extracts due to restricted diffusion and contact with microbial cells.

A significant improvement in antibacterial effectiveness is noted for textiles treated with hydrogels containing AgNPs. AgNPs synthesised from aqueous hypericin extracts demonstrate nearly total microbial reduction, achieving 99.1% efficacy against S. aureus and 97.8% against E. coli. This exceptional performance demon-

strates the combined antibacterial actions of silver nanoparticles, encompassing membrane rupture, protein denaturation, DNA binding, and the continuous release of Ag^+ ions. The little reduced activity against C. albicans (88.3%) aligns with the enhanced durability of fungal cell walls; it still signifies a very efficient antifungal response. AgNPs synthesised with chamomile extracts have comparably high antibacterial activity, while somewhat inferior to that of hypericin-based systems, underscoring the impact of nanoparticle capping agents on antimicrobial efficacy.

AgNPs synthesised in sesame oil exhibit considerably reduced, although still significant, antibacterial decreases. The diminished efficiency is likely attributable to suboptimal nanoparticle dispersion and partial occlusion of silver surfaces by hydrophobic oil constituents, which restricts Ag^+ ion availability and interaction with microbial cells. Nonetheless, the documented decreases affirm that silver nanoparticles continue to be the primary antibacterial agent, even in oil-based systems.

Table 6 illustrates that the antibacterial efficacy is ranked as follows: AgNP-containing hydrogels > extract-loaded hydrogels > plain hydrogel > untreated fabric. The findings underscore the significant synergistic interaction between silver nanoparticles and plant-derived bioactives when encapsulated in a biocompatible hydrogel matrix. The extensive antimicrobial efficacy against Gram-positive bacteria, Gram-negative bacteria, and fungi highlights the potential of these treated nonwoven textiles as sophisticated wound dressings that can prevent infection while ensuring biocompatibility and multifunctionality.

Table 6: Antimicrobial reduction of untreated and treated nonwoven fabric with different hydrogel formulations

Fabric	Antimicrobial Reduction (R; %)		
	S. aureus	**E. coli**	**C. albicans**
Untreated Fabric	**0**	0	0
Gel only	42 ± 2.1	31 ± 2.7	18 ± 2.2
Ethanolic Hypericin	71 ± 4.1	63 ± 2.4	54 ± 3.6
Methanolic Chamomile	66 ± 2.8	58 ± 4.1	49 ± 4.1
Sesam oil	51 ± 3.1	43 ± 3.2	36 ± 2.5
AgNPs-Aqueous Hypericin	**99.1 ± 0.4**	**97.8 ± 0.6**	**88.3 ± 1.2**
AgNPs-Aqueous Chamomile	96.5 ± 0.7	95.1 ± 0.8	83.4 ± 1.4
AgNPs-Sesame oil	81 ± 2.6	73 ± 2.5	66 ± 2.8

3.6.3. Morphological behaviour of coated fabric

Figure 11 displays SEM micrographs of the surface morphology of the nonwoven fabric before and after coating with the O-CMC/Ox-Alg hydrogel systems incorporating diverse bioactive agents and AgNPs. The untreated nonwoven fabric (Figure 11a) displays a conventional loose fibrous structure including smooth, unblemished fibres and substantial inter-fiber spaces, indicative of inert textile substrates with little surface functioning. The open shape accounts for the lack of intrinsic bioactivity and little protein adsorption seen in the untreated cloth.

After the hydrogel coating, a significant alteration in surface morphology is seen in all treated samples. Fabrics coated with O-CMC/Ox-Alg infused with hypericin (Figure 11b) and chamomile (Figure 11c) exhibit homogeneous hydrogel coverage across the fibre surfaces, resulting in a continuous and rather smooth layer that connects neighbouring fibres. The incomplete occupancy of inter-fiber pores signifies successful hydrogel infiltration and adherence, attributable to robust hydrogen bonding and electrostatic interactions between the polysaccharide matrix and the cellulose-based textile fibres. This uniform coating is strongly associated with the improved antioxidant activity and antibacterial efficacy of these samples, since the bioactive chemicals are uniformly dispersed over the fabric surface.

Conversely, the sesame oil–infused hydrogel covering (Figure 11d) displays a more heterogeneous morphology, characterised by localised agglomerates and less surface uniformity. Hydrophobic oil domains disturb the continuity of the hydrogel layer, leading to microphase separation and uneven surface characteristics. This structural variability aligns with the more diminished antioxidant activity and antibacterial effectiveness of sesame oil-treated textiles, alongside their increased protein adsorption, facilitated by exposed hydrophobic areas.

Fabrics coated with hydrogels containing AgNPs have significantly different surface characteristics. The AgNPs/Hypericin (Figure 11e) and AgNPs/Chamomile (Figure 11f) coatings exhibit dense, compact hydrogel layers with nanoscale particles uniformly dispersed on the fibre surfaces. The decreased pore visibility and enhanced surface roughness indicate effective nanoparticle integration within the hydrogel matrix and robust interfacial interactions. This compact architecture enhances the observed high antibacterial efficacy, since the

proximity between AgNPs and the fabric surface promotes continuous Ag^+ release and direct microbial interaction. Conversely, the AgNPs/Sesame oil-coated fabric (Figure 11g) demonstrates a less uniform dispersion of nanoparticles and localised aggregation, indicating less compatibility between the hydrophobic oil phases and the hydrophilic hydrogel matrix. This structural constraint elucidates the somewhat diminished antibacterial and antioxidant efficacy of this formulation.

The SEM data indicate that hydrogel composition and included agents significantly affect coating uniformity, porosity, and surface roughness. Homogeneous, well-adhered hydrogel layers—especially those including polar plant extracts and AgNPs—yield compact, bioactive surfaces that enhance the antioxidant and antibacterial efficacy of the treated textiles. These findings indicate that tailored hydrogel coating alters textile shape and significantly influences the functional performance of advanced wound dressing materials.

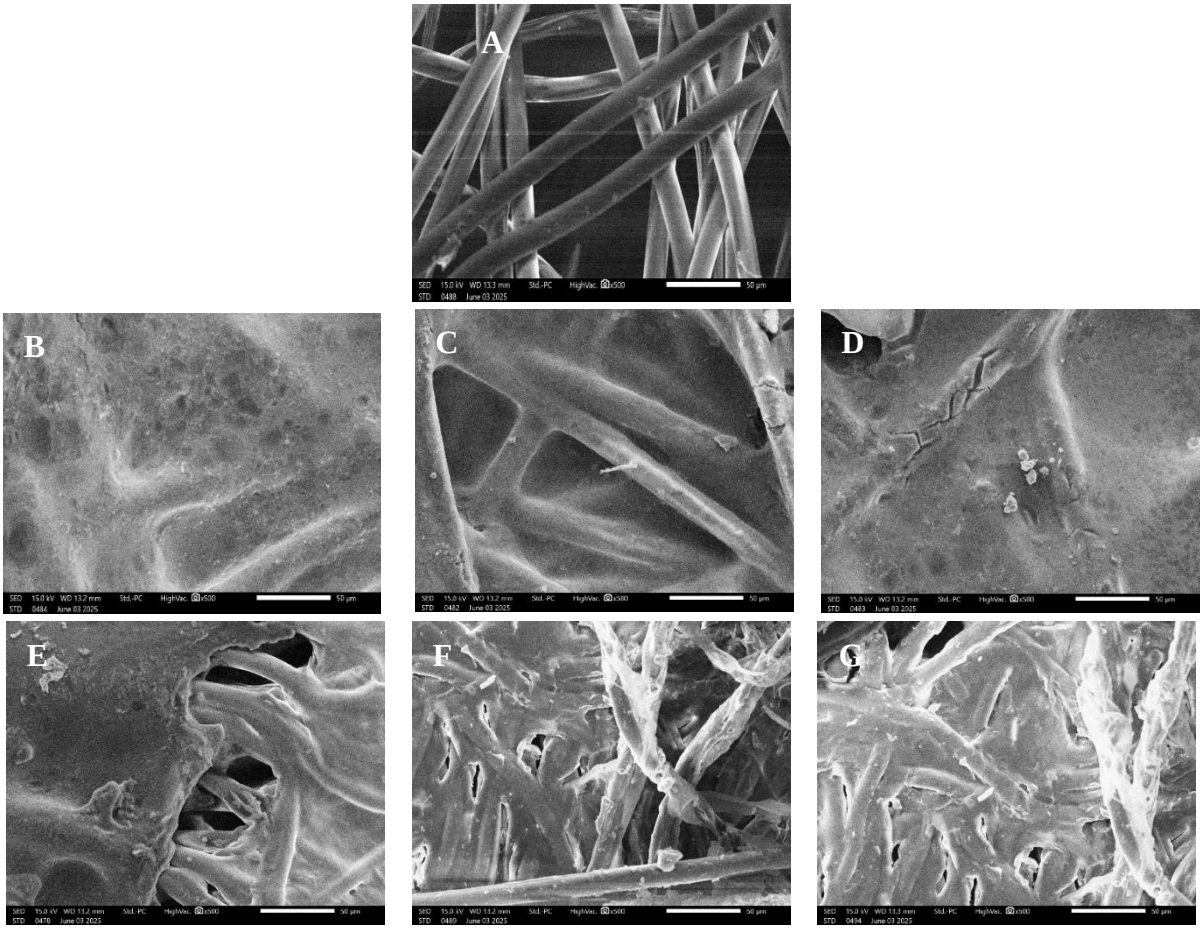

Figure 11: SEM micrographs of nonwoven fabrics before and after coating with hydrogel coating

(a) untreated nonwoven fabric; fabrics coated with O-CMC/Ox-Alg as follow (B) Hypericin (20%), (C) Chamomile (20%), (D) Sesam oil (15%), (E) AgNPs/Hypericin (15%), (F) AgNPs/Chamomile (15%), and (G) AgNPs/Sesam oil (15%)

3.6.4. Release profile

Figure 12 depicts the cumulative release patterns of bioactive compounds from nonwoven wound dressings covered with O-CMC/Ox-Alg (3:2) hydrogels infused with various natural extracts and their AgNP-embedded equivalents. All formulations have a distinct biphasic release pattern, comprising an initial quick release phase succeeded by a slower, sustained release stage, which is particularly advantageous for wound-healing applications necessitating immediate therapeutic action and extended efficacy.

Hypericin-loaded hydrogels exhibit a significant burst release within the initial 0.25–1 hour, with around 49% release for hypericin alone and a notably elevated release of around 69–73% for AgNPs/hypericin systems. The swift initial release is due to loosely attached or surface-associated hypericin molecules in the hydrogel matrix, enabled by the comparatively hydrophilic characteristics of the O-CMC/Ox-Alg network. The addition

of AgNPs enhances early release, probably due to localised disruption of polymer chain packing and augmented free volume at nanoparticle–polymer interfaces. After this first phase, hypericin release progressively nears a plateau, attaining around 89% for hypericin alone and around 87% for AgNP-loaded systems at 8 hours, signifying diffusion-controlled transport from the hydrogel interior and stable retention of the residual fraction.

Hydrogels infused with chamomile have a more regulated and gradual release profile in comparison to hypericin. The first release at 0.25 hours is constrained to around 12–24%, indicating enhanced interactions between chamomile polyphenols and the polysaccharide network via hydrogen bonding and electrostatic interactions. A gradual release is noted, achieving around 77% for chamomile alone and around 69% for chamomile combined with AgNPs at 8 hours. The addition of AgNPs notably increases initial release while marginally inhibiting total cumulative release, indicating partial adsorption or coordination of chamomile components onto AgNP surfaces, which hinders their diffusion in subsequent phases.

Formulations based on sesame oil exhibit the slowest initial release, with just ~4–8% released during the first 0.25 hours, due to the hydrophobic characteristics of sesame oil and its restricted affinity for the aqueous hydrogel domains. Nonetheless, a persistent and significant escalation in release transpires with time, especially for sesame oil alone, attaining around 97% at 8 hours. This protracted yet comprehensive release signifies the progressive diffusion of oil through expanded hydrogel channels created when the network relaxes and assimilates water. The AgNPs/sesame oil system demonstrates a more controlled release (~87% at 8 h), attributable to the partial immobilisation of oil droplets inside AgNP-associated domains and a denser local microstructure that restricts oil mobility.

AgNP-loaded systems often demonstrate a more rapid initial release but somewhat reduced ultimate release percentages compared to their extract-only equivalents. This behaviour highlights the dual function of AgNPs as structural modifiers of the hydrogel network and as interaction sites for bioactive compounds. The regulated release profiles obtained with O-CMC/Ox-Alg (3:2) hydrogels demonstrate that the optimised Schiff-base crosslinked network offers enough mechanical integrity while preserving adjustable diffusional channels for various bioactive agents.

The release behaviour illustrated in Figure 12 underscores the adaptability of the engineered hydrogel-coated wound dressings. The first therapeutic burst—essential for fast antibacterial and antioxidant effects—coupled with continuous release, facilitates extended wound protection and healing. Hypericin- and AgNP-containing systems are particularly promising candidates, providing a balanced release profile consistent with their previously reported high antimicrobial and antioxidant efficacy, thus enhancing the appropriateness of these multifunctional hydrogel coatings for advanced wound-care applications.

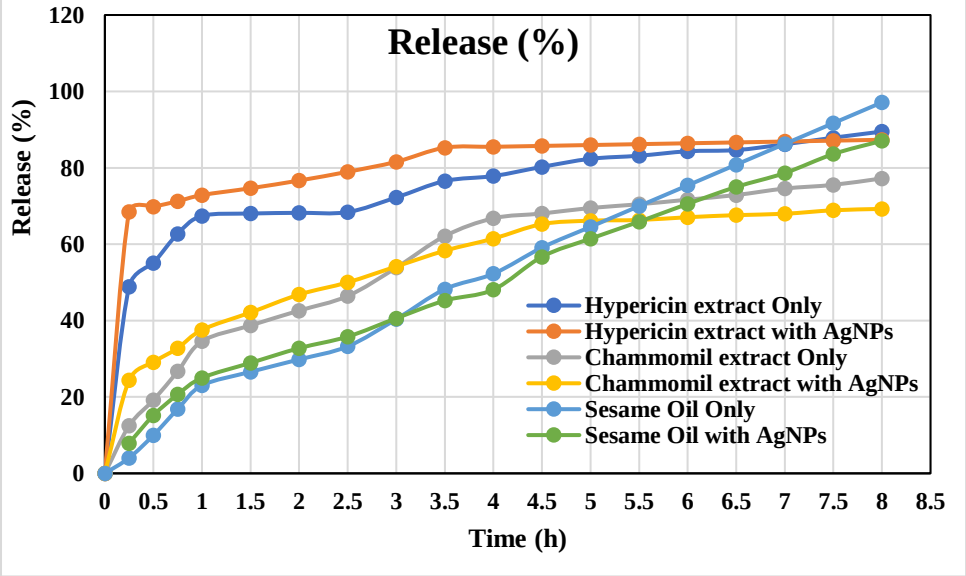

Figure 12: Release profile of bioactive extract from nonwoven wound bandage coated with various hydrogels O-CMC/Ox-Alg (3:2) with different bioactive materials as: Hypericin (20%), Chamomile (20%), Sesam oil (15%), AgNPs/Hypericin (15%), AgNPs/Chamomile (15%), and AgNPs/Sesam oil (15%)

4. Concolusion

This study successfully developed a multifunctional bioactive wound dressing utilising hydrogel-coated cotton nonwoven fabrics, incorporating chemically modified natural polymers and plant-derived silver nanoparticles, specifically tailored to meet the intricate demands of pressure ulcer healing. Oxidised sodium alginate and O-carboxymethyl chitosan were systematically chosen and chemically modified to create self-crosslinked hydrogels by dynamic Schiff-base chemistry, facilitating injectable, in situ gelation and durable coating on textile substrates. The oxidation level of alginate was meticulously regulated to preserve mechanical integrity while ensuring adequate aldehyde functionality for efficient crosslinking, with intermediate oxidation levels demonstrating excellent hydrogel performance.

A thorough physicochemical characterisation validated the effective alteration of the polymer and the production of the hydrogel. FTIR tests confirmed the oxidation of alginate and the creation of imine bonds between the aldehyde groups of Ox-Alg and the amino groups of O-CMC, whereas nitrogen elemental analysis quantitatively indicated a gradual consumption of amines and an increase in imine density with varying polymer ratios. The computed molar density of Schiff-base crosslinks indicated that intermediate compositions (O-CMC/Ox-Alg = 3:2 and 2:3) attained the most efficient network structure, corresponding with reduced gelation periods, optimal swelling characteristics, and improved structural integrity. These attributes are essential for pressure ulcer dressings, which must adapt to variable wound shapes while preserving integrity under extended mechanical stress.

Functional performance assessments further indicated that hydrogel composition significantly affects biological behaviour. Swelling investigations verified sufficient fluid absorption capacity without excessive enlargement, enabling effective exudate management and limiting maceration of adjacent tissue. Protein adsorption studies demonstrated adjustable surface bioactivity, with particular formulations facilitating moderate protein binding—beneficial for cell adhesion and tissue regeneration—while AgNP-containing systems showed less nonspecific adsorption, presumably due to antimicrobial surface properties.

The integration of plant-derived bioactive extracts (hypericin, chamomile, and sesame oil) together with their respective green-synthesized AgNPs markedly improved the therapeutic efficacy of the hydrogel-coated dressings. The antioxidant activity significantly enhanced with bioactive loading, especially in hypericin- and chamomile-based systems, therefore effectively alleviating oxidative stress, a critical pathogenic element in chronic pressure ulcers. SEM analysis verified consistent hydrogel application and successful incorporation of bioactive compounds and nanoparticles into the fibrous textile matrix, maintaining fabric porosity and elasticity.

Antimicrobial evaluations revealed a robust and synergistic antibacterial and antifungal effectiveness. Extract-only hydrogels yielded considerable microbial decrease, but AgNP-loaded formulations attained nearly total suppression of S. aureus and E. coli, together with significant inhibition of C. albicans. The extensive antibacterial efficacy is especially vital for pressure ulcers, which are prone to polymicrobial infections and biofilm development.

Release trials further confirmed the appropriateness of the designed dressings for chronic wound management. All formulations demonstrated a biphasic release profile, with an initial burst release—crucial for prompt microbial control and inflammation alleviation—followed by a sustained release of bioactive chemicals over many hours. Hydrogels containing AgNPs regulated release kinetics, providing improved early-stage therapeutic availability while ensuring sustained efficacy, thereby minimising the necessity for frequent dressing changes.

The results together indicate that the proposed bioactive hydrogel-coated cotton dressings effectively combine mechanical compliance, moisture management, antioxidant protection, controlled medication release, and strong antibacterial action in a single platform. The synergistic integration of chemically altered biopolymers, botanical extracts, and green-synthesized silver nanoparticles presents a promising, biocompatible, and sustainable approach for the management of progressive pressure ulcers. This technology demonstrates significant potential to expedite healing, diminish infection risk, and enhance patient comfort, establishing it as a promising contender for advanced wound care applications.

5. Prospective Outlooks

The current study illustrates the significant potential of bioactive hydrogel-coated cotton dressings in managing pressure ulcers; several opportunities for further development and optimisation persist. Subsequent research must concentrate on in vivo assessments employing clinically pertinent pressure ulcer models to corroborate the identified antimicrobial, antioxidant, and controlled-release characteristics under physiological

wound conditions, encompassing dynamic exudate flow, bacterial biofilm development, and recurrent mechanical loading. Prolonged biocompatibility and biodegradation investigations are crucial to validate the safety of extended hydrogel exposure to compromised skin and underlying tissues.

From a materials design standpoint, precise manipulation of alginate oxidation degree and polymer molecular weight might be investigated to customise breakdown rates, mechanical strength, and drug-release kinetics for various ulcer stages. The inclusion of further bioactive signals, such as growth factors, angiogenic peptides, or oxygen-releasing compounds, may further augment tissue regeneration and vascularization in ischaemic pressure ulcers. Furthermore, the dynamic Schiff-base network presents prospects for self-healing and stimuli-responsive behaviour, which might be utilised to create intelligent dressings that respond to pH variations, enzyme activity, or infection-related indicators.

Considerations regarding scale-up and production also require attention. The eco-friendly synthesis of silver nanoparticles (AgNPs) utilising plant extracts and the aqueous processing of biopolymers establishes a robust basis for economical and sustainable manufacturing. Subsequent research should evaluate batch-to-batch repeatability, sterilisation compatibility, and shelf stability to facilitate industrial use. Moreover, the use of new textile technologies, such as multilayer or gradient dressings, might enhance efficacy in intricate chronic wound settings.

6. Clinical Significance

Pressure ulcers provide a considerable therapeutic problem, especially in immobilised, aged, and critically sick patients, since delayed healing, infection, and oxidative stress significantly elevate morbidity and healthcare expenses. The hydrogel-coated cotton dressings created in this study directly fulfil essential clinical needs for optimal pressure ulcer therapy, including moisture regulation, antibacterial defence, oxidative stress mitigation, and prolonged therapeutic administration.

The fast yet manageable gelation properties provide conformal coating of wound surfaces and textile substrates, enhancing dressing adherence and patient comfort while reducing leakage or displacement. Equilibrated swelling characteristics facilitate effective absorption of wound exudate without undue enlargement, hence minimising the danger of periwound maceration. The integration of plant-derived bioactive compounds and silver nanoparticles delivers extensive antimicrobial efficacy, effectively safeguarding against prevalent pressure-ulcer pathogens, including Staphylococcus aureus, Escherichia coli, and Candida albicans, while potentially diminishing dependence on systemic antibiotics.

The documented antioxidant activity and sustained release characteristics are especially pertinent for chronic pressure ulcers, where extended inflammation and oxidative harm hinder recovery. The integration of natural antioxidants with regulated AgNP administration in the proposed dressings fosters a localised wound environment that promotes tissue regeneration and infection management. Moreover, the utilisation of biocompatible, renewable polymers and green-synthesized nanoparticles corresponds with the growing clinical demand for safe, sustainable, and patient-centric wound care treatments.

The findings indicate that bioactive hydrogel-coated dressings possess significant potential to serve not merely as passive wound coverings but as active therapeutic platforms, capable of enhancing healing, diminishing infection rates, and improving the quality of life for patients with pressure ulcers. Upon additional preclinical and clinical validation, this approach may signify a significant breakthrough in contemporary wound-care practices.

7. Fund

The authors declare that there is no fund.

8. Conflict of interest

The authors declare that there is no conflict of interest.

9. Declaration section

The datasets used and/or analysed during the current study are available from the corresponding author upon reasonable request.

10. Acknowledgments

The authors are grateful to acknowledge Benha University, Faculty of Applied Arts, Benha, Egypt. Furthermore, the authors are grateful to acknowledge the Central Labs Services (CLS) and Centre of Excellence for Innovative Textiles Technology (CEITT) in Textile Research and Technology Institute (TRTI), National Research Centre (NRC) for the facilities provided.

1. References

[1]. M. Tanwar, A. Rani, N. Gautam, S. Talegaonkar, R.K. Gupta, Essential oils loaded carboxymethylated cassia fistula gum-based novel hydrogel films for wound healing, International Journal of Biological Macromolecules 278 (2024) 134682.

[2]. J.C. Dumville, J. Webster, D. Evans, L. Land, Negative pressure wound therapy for treating pressure ulcers, The Cochrane database of systematic reviews (5) (2015) Cd011334.

[3]. J.S. Mervis, T.J. Phillips, Pressure ulcers: Pathophysiology, epidemiology, risk factors, and presentation, Journal of the American Academy of Dermatology 81(4) (2019) 881–890.

[4]. C. Zhang, S. Zhang, B. Wu, K. Zou, H. Chen, Efficacy of different types of dressings on pressure injuries: Systematic review and network meta-analysis, Nursing open 10(9) (2023) 5857–5867.

[5]. S.N. Sinha, B. Free, O. Ladlow, The art and science of selecting appropriate dressings for acute open wounds in general practice, Australian Journal of General Practice 51(11) (2022) 827–830.

[6]. P. Kolimi, S. Narala, D. Nyavanandi, A.A.A. Youssef, N. Dudhipala, Innovative treatment strategies to accelerate wound healing: Trajectory and recent advancements, Cells 11(15) (2022) 2439.

[7]. M.J. Westby, J.C. Dumville, M.O. Soares, N. Stubbs, G. Norman, Dressings and topical agents for treating pressure ulcers, The Cochrane database of systematic reviews 6(6) (2017) Cd011947.

[8]. Y. Wang, D. Xiao, H. Yu, Y. Zhong, L. Zhang, X. Sui, B. Wang, X. Feng, H. Xu, Z. Mao, Composite hydrogel based oxidated sodium carboxymethyl cellulose and gelatin loaded carboxymethylated cotton fabric for hemostasis and infected wound treatment, International Journal of Biological Macromolecules 224 (2023) 1382–1394.

[9]. M. Tauseef, F. Azam, Y. Iqbal, S. Ahmad, F. Ahmad, R. Masood, S.R. Habib, A. Rasheed, M.S. Zafar, A. Salam, Development and evaluation of silver-infused biopolymer coated cotton wound dressings as possible wound healing material, Heliyon 10(19) (2024).

[10]. S.S.M. Abdel Wahab, H.A.A. Atallah, Y.D.M. Saleh, R.E. Glal El-Den, A.G. Hassabo, Challenges and unsustainable practices in the apparel sector, J. Text. Color. Polym. Sci. 23(1) (2026) 43–48.

[11]. Z.S. Beltagy, H. Ghazal, A.G. Hassabo, Enhancing dyeability and smart functionality of cellulosic and blended textiles using various natural keratin extracts, Egy. J. Chem. (2026).

[12]. S.A. Ebrahim, M.M. Mosaad, A.G. Hassabo, H.A. Othman, Residual of natural protein- and polysaccharide-based biopolymers from livestock and marine wastes for sustainable textile processing and functional finishing, Egy. J. Chem. (2026).

[13]. M.A. Eida, H.S. Soliman, M.A. Alkaramani, I.G. Elbadwy, Z.A. Awad, A.G. Hassabo, The impact of modern printing techniques on the attractiveness of advertisements, J. Text. Color. Polym. Sci. 23(1) (2026) 27–34.

[14]. E. El-Sayed, H. Othman, E. Abd El-Aziz, A.G. Hassabo, Development of new azo dyes based on natural plant extracts (peanut red skin and onion peel) for dyeing and finishing of textile fabrics using vari-ous amino aromatic compounds, Egy. J. Chem. (2026) –.

[15]. H.I. Elhefnawy, M.A. Saada, S.T. Abdelkareem, Y.A. Elemam, R.A. Subaih, A.G. Hassabo, Color theory and semiotics: Exploring the relationship between visual semiotics and color, J. Text. Color. Polym. Sci. 23(1) (2026) 9–15.

[16]. S.M.M.E. Elrys, S. Elaraby, K. Mahmoud, R. Abdalmagid, M. Abdalatif, M. Magdy, M. Tarek, F.F. El-Habiby, A.G. Hassabo, Impact of polyester/cotton fabric composition on the controlled release of amoxicillin and ginger extract for sustainable wound dressing applications, Egy. J. Chem. (2026).

[17]. M.N. Elshamy, H. Ghazal, A.G. Hassabo, Sustainable dyeing of cotton and polyester fabrics using agricultural-waste-derived carboxymethyl cellulose and natural colourants: Optimisation, performance evaluation, and functional finishing, Egy. J. Chem. (2026).

[18]. J. Gaukhar, B.R. Taussarova, A. Burkitbay, A.G. Hassabo, Enhancement of fire resistance in cotton/polyester and cotton/linen blends using sol-gel derived silicate/phosphate coatings, Egy. J. Chem. 69(3) (2026) 37– 46.

[19]. N.A. Ibrahim, A.S. Montaser, A.L. Mohamed, Chapter 7 - environmentally sound and sustainable approaches for modification of cellulosic materials and fibers, in: M. Montazer, A. Mianehro (Eds.), Cellulose science and technology, Elsevier2026, pp. 129–211.

[20]. M.A. Mohammed, E.a. Ahmed, A.E. Fahmy, A.G. Hassabo, Hand weaving tools and materials, J. Text. Color. Polym. Sci. 23(1) (2026) 35–41.

[21]. H.M.Y. Okda, E.R. Sheha, F. Zahran, M.A. Yousef, T.I. Shaheen, A.G. Hassabo, Development of multilayered polymer-baso(4) composites for flexible and efficient lead-free x-ray shielding, Scientific Reports (2026).

[22]. H.M.Y. Okda, E.R. Sheha, F. Zahran, M.A. Yousef, T.I. Shaheen, A.G. Hassabo, Development of multilayered polymer-baso4 composites for flexible and efficient lead-free x-ray shielding, Scientific Reports 16(1) (2026) 6719.

[23]. E. Reda, H. Ghazal, A.G. Hassabo, H.A. Othman, Natural residual resources for sustainable and eco-efficient textile wet pro-cessing, Egy. J. Chem. (2026).

[24]. F. Saad, M.M. Mosaad, A.G. Hassabo, H.A. Othman, Eco-friendly polyurethane binders from castor and linseed oil polyols reinforced with chitosan for enhanced pigment printing performance and mechanical properties of textile fabrics, Egy. J. Chem. (2026).
[25]. F. Saad, M.M. Mosaad, H. Othman, A.G. Hassabo, A critique on pigment printing techniques, J. Text. Color. Polym. Sci. 23(1) (2026) 135–149.
[26]. M.A. Saada, S.T. Abdelkareem, Y.A. Elemam, R.A. Subaih, H.I. Elhefnawy, A.G. Hassabo, Evolution and importance of materials in industrial design, J. Text. Color. Polym. Sci. 23(1) (2026) 1–7.
[27]. M. Zayed, E. Abd El-Aziz, H. Ghazal, A.G. Hassabo, H. Othman, Phase change materials (pcm) for sustainable textile materials: Design, characteristic, performance and application, J. Text. Color. Polym. Sci. 23(1) (2026) 121–134.
[28]. E.A. Zein El dein, S.M. Ali, E.H.s. Ghoneim, A.G. Hassabo, Enamel materials and its relation with jewellery and metal products field, J. Text. Color. Polym. Sci. 23(1) (2026) 49–58.
[29]. N.A. Abd El-Salam, H. Othman, A.G. Hassabo, A.R. Shahin, Rheological properties and printing performance of neem gum as an eco-friendly thickening agent for textile printing, Egy. J. Chem. 69(3) (2026) 549–564.
[30]. F.M. Ahmed, E.-S. El-Shahat, H. Othman, A.L. Mohamed, Chemical modification of natural dyes: Enhancing performance and sustainability in textile applications, Egy. J. Chem. 69(3) (2026) 399–415.
[31]. O.G. Allam, A.L. Mohamed, E.M. Swielam, Al_2o_3 nanoparticles and mint oil composites for textile treatment enhancement, Egy. J. Chem. 69(5) (2026) 393–402.
[32]. S.A. Ebrahim, M.M. Mosaad, H.A. Othman, A.G. Hassabo, Clay minerals in textile engineering: Synthesis, characterization and applications of polymer-clay nanocomposites for enhanced fabric performance, Egy. J. Chem. 69(3) (2026) 463–503.
[33]. F.M. Ahmed, E.-S. El-Shahat, H.A. Othman, A.L. Mohamed, Chemical and physical modification strategies of synthetic fibers to enhance dye uptake and color performance, Egy. J. Chem. (Accept 2026).
[34]. F.M. Ahmed, E.-S. El-Shahat, H.A. Othman, A.L. Mohamed, Chemical modification of betalain extracts from beta vulgaris via azo dye synthesis using aniline-based aromatic amines for enhanced dye uptake and color performance, Egy. J. Chem. (Accept 2026).
[35]. S.M.M.E. Elrys, S. Elaraby, K. Mahmoud, R. Abdalmagid, M. Abdalatif, M. Magdy, M. Tarek, F.F. El-Habiby, A.G. Hassabo, Influence of polyester/cotton fabric composition on ultraviolet protection factor following treatment with znonps embedded in cellulosic and pro-teinaceous from waste substrates, Egy. J. Chem. (Accept 2026).
[36]. A.G. Hassabo, H.M.Y. Okda, E.R. Sheha, R.F. El-Newashy, A.L. Mohamed, Development of eco-friendly x-ray protective cotton fabrics based on pectin/barium sulfate composites as a non-lead shielding material, Egy. J. Chem. (Accept 2026).
[37]. A.L. Mohamed, A.G. Hassabo, Amphiphilic biopolymers in textiles and drug delivery: Functional roles of chitosan and starch in controlled release and smart fabric applications, Egy. J. Chem. (Accept 2026).
[38]. A. Sediek, M.M. Mosaad, H.A. Othman, A.L. Mohamed, Bioactive hydrogel-coated cotton dressings based on chemically modified biopolymers and plant-derived silver nanoparticles for enhanced pressure ulcer healing, Egy. J. Chem. (Accept 2026).
[39]. A. Sediek, M.M. Mosaad, H.A. Othman, A.L. Mohamed, Advances in biopolymer-based medical textiles: Properties, functional performance, and emerging applications, Egy. J. Chem. (Accept 2026).
[40]. M.Y. Soliman, A.G. Hassabo, H.A. Othman, Improvement of upholstery fabric printability and functional efficiency by natural extract–metal nanoparticle treatments for self-cleaning and flame-retardant properties, Egy. J. Chem. (Accept 2026).
[41]. M.M. Ragab, H.A. Othman, A.G. Hassabo, An overview of printing textile techniques, Egy. J. Chem. 65(8) (2022) 749 – 761.
[42]. M.M. Ragab, H. Othman, A.J.E.J.o.C. Hassabo, An overview of printing textile techniques, 65(8) (2022) 749–761.
[43]. G.A. El-Sayed, H. Othman, A.G. Hassabo, An overview on the eco-friendly printing of jute fabrics using natural dyes, J. Text. Color. Polym. Sci. 18(2) (2021) 239–245.
[44]. D.M. Hamdy, A.G. Hassabo, H. Othman, Recent use of natural thickeners in the printing process, J. Text. Color. Polym. Sci. 18(2) (2021) 75–81.
[45]. H. Ghazal, N. Khaleed, S. Shaker, A.G. Hassabo, An overview of the dyeing process of lyocell fabric and its blends, J. Text. Color. Polym. Sci. 21(1) (2024) 49–62.
[46]. H. Othman, S.S. Moawaed, R. Abd El-Rahman, A. abdelraouff, S.S. El-Desoky, G.A. El-Bahrawy, H.A. Ezat, A.G. Hassabo, Various printing techniques of viscose/polyester fabric to enhancing its performance properties, J. Text. Color. Polym. Sci. 20(2) (2023) 285–295.
[47]. H. Othman, H.A. Ezat, S.S. Moawaed, R. Abd El-Rahman, A. abdelraouff, S.S. El-Desoky, G.A. El-Bahrawy, A.G. Hassabo, Various printing techniques of silk fabric to enhancing its performance properties, J. Text. Color. Polym. Sci. 21(1) (2024) 23–32.
[48]. H. Othman, R.H. Abd El-Rahman, A.A. Mokhtar, S.S. El-Desoky, G.A. El-Bahrawy, H.A. Ezat, S.S. Moawaed, A.G. Hassabo, Various printing techniques of intelligent lyocell fabric to enhancing its performance properties, Egy. J. Chem. 66(12) (2023) 413 – 419.
[49]. H. Othman, A. abdelraouff, S.S. El-Desoky, G.A. El-Bahrawy, H.A. Ezat, S.S. Moawaed, R. Abd El-Rahman, A.G. Hassabo, Various printing techniques of cotton/polyester blended fabrics to enhancing its performance properties, J. Text. Color. Polym. Sci. 20(2) (2023) 277–284.
[50]. A. AlAshkar, A.G. Hassabo, Recent use of natural animal dyes in various field, J. Text. Color. Polym. Sci. 18(2) (2021) 191–210.

[51]. M.M. Ragab, A.G. Hassabo, Various uses of natural plants extracts for functionalization textile based materials, J. Text. Color. Polym. Sci. 18(2) (2021) 143–158.
[52]. D.M. Hamdy, H.A. Othman, A.G. Hassabo, Various natural dyes from different sources, J. Text. Color. Polym. Sci. 18(2) (2021) 171–190.
[53]. D.M. Hamdy, H.A. Othman, A.G. Hassabo, Various natural dyes using plant palette in coloration of natural fabrics, J. Text. Color. Polym. Sci. 18(2) (2021) 121–141.
[54]. M.M. Ragab, A.G. Hassabo, H.A. Othman, An overview of natural dyes extraction techniques for valuable utilization on textile fabrics, J. Text. Color. Polym. Sci. 19(2) (2022) 137–153.
[55]. A.A. Nada, A.G. Hassabo, A.L. Mohamed, M.M. Mounier, N.Y. Abou Zeid, Liposomal microencapsulation of rodent-repelling agents onto jute burlaps: Assessment of cytotoxicity and rat behavioral test, Journal of Applied Pharmaceutical Science 6(8) (2016) 142–150.
[56]. M.S. Kamal, E. Mahmoud, A.G. Hassabo, M.M. Eid, Effect of some construction factors of bi-layer knitted fabrics produced for sports wear on resisting ultraviolet radiation, Egy. J. Chem. 63(11) (2020) 4369 – 4378.
[57]. A. Aboelnaga, S. Shaarawy, A.G. Hassabo, Polyaconitic acid/functional amine/azo dye composite as a novel hyper-branched polymer for cotton fabric functionalization, Colloids Surf. B: Biointer. 172 (2018) 545–554.
[58]. T. Maver, S. Hribernik, T. Mohan, D.M. Smrke, U. Maver, K. Stana-Kleinschek, Functional wound dressing materials with highly tunable drug release properties, RSC advances 5(95) (2015) 77873–77884.
[59]. L. Wang, D. Li, Y. Shen, F. Liu, Y. Zhou, H. Wu, Q. Liu, B. Deng, Preparation of centella asiatica loaded gelatin/chitosan/nonwoven fabric composite hydrogel wound dressing with antibacterial property, International Journal of Biological Macromolecules 192 (2021) 350–359.
[60]. Z. Doozandeh, S. Saber-Samandari, A. Khandan, Preparation of novel arabic gum-c6h9no biopolymer as a bedsore for wound care application, Acta Medica Iranica (2020) 520–530.
[61]. V. Singh, T. Marimuthu, M.M. Makatini, Y.E. Choonara, Biopolymer-based wound dressings with biochemical cues for cell-instructive wound repair, Polymers 14(24) (2022) 5371.
[62]. L. Upadhyaya, J. Singh, V. Agarwal, R.P. Tewari, Biomedical applications of carboxymethyl chitosans, Carbohydrate Polymers 91(1) (2013) 452–466.
[63]. M. Ji, J. Li, Y. Wang, F. Li, J. Man, J. Li, C. Zhang, S. Peng, S. Wang, Advances in chitosan-based wound dressings: Modifications, fabrications, applications and prospects, Carbohydrate Polymers 297 (2022) 120058.
[64]. L. Wang, R. Guo, X. Liang, Y. Ji, J. Zhang, G. Gai, Z. Guo, Preparation and antioxidant activity of new carboxymethyl chitosan derivatives bearing quinoline groups, Marine Drugs 21(12) (2023) 606.
[65]. H. Wang, X. Chen, Y. Wen, D. Li, X. Sun, Z. Liu, H. Yan, Q. Lin, A study on the correlation between the oxidation degree of oxidized sodium alginate on its degradability and gelation, Polymers 14(9) (2022) 1679.
[66]. S. Reakasame, A.R. Boccaccini, Oxidized alginate-based hydrogels for tissue engineering applications: A review, Biomacromolecules 19(1) (2018) 3–21.
[67]. W. Wang, M. Liu, M. Shafiq, H. Li, R. Hashim, E.L.N. Mohamed, E.L.H. Hany, Y. Morsi, X. Mo, Synthesis of oxidized sodium alginate and its electrospun bio-hybrids with zinc oxide nanoparticles to promote wound healing, International Journal of Biological Macromolecules 232 (2023) 123480.
[68]. X. Kong, L. Chen, B. Li, C. Quan, J. Wu, Applications of oxidized alginate in regenerative medicine, Journal of materials chemistry B 9(12) (2021) 2785–2801.
[69]. S. Özdemir, S.Y. Bostanabad, A. Parmaksız, H.C. Canatan, Combination of st. John's wort oil and neem oil in pharmaceuticals: An effective treatment option for pressure ulcers in intensive care units, Medicina (Kaunas, Lithuania) 59(3) (2023).
[70]. U. Wölfle, G. Seelinger, C.M. Schempp, Topical application of st. John's wort (hypericum perforatum), Planta medica 80(2-3) (2014) 109–20.
[71]. Y. Sotirova, D. Vankova, O. Tasinov, S. Stoeva, M. Hristova, I. Iliev, S. Georgieva, Y. Kiselova-Kaneva, V. Andonova, Bigel formulations of st. John’s wort extract in wound healing: Toxicological aspects, Biotechnology & Biotechnological Equipment 37(1) (2023) 2263570.
[72]. T. El-Elimat, H.S. El-Qaderi, W.M. Hananeh, M.M. Abu AlSamen, A.H. Al Sharie, M.A. Alshehabat, M. Al-Gharaibeh, F.Q. Alali, Evaluation of the wound healing potential of hypericum triquetrifolium turra: An experimental animal study and histopathological examination, Scientia Pharmaceutica 91(1) (2023) 16.
[73]. A. Yücel, Y. Kan, E. Yesilada, O. Akın, Effect of st. John's wort (hypericum perforatum) oily extract for the care and treatment of pressure sores; a case report, Journal of ethnopharmacology 196 (2017) 236–241.
[74]. Z.S. Hamedi, A. Manafi, S.-S. Hashemi, D. Mehrabani, A. Seddighi, N. Tanideh, M.J.W.J.o.P.S. Mokhtari, Healing effect of hypericum perforatum in burn injuries, 13(3) (2024) 57.
[75]. A. Anis, A. Sharshar, S. El Hanbally, Y. Sadek, A novel organic composite accelerates wound healing: Experimental and clinical study in equine, Journal of Equine Veterinary Science 99 (2021) 103406.
[76]. M. Jarrahi, A.A. Vafaei, A.A. Taherian, H. Miladi, A. Rashidi Pour, Evaluation of topical matricaria chamomilla extract activity on linear incisional wound healing in albino rats, Natural product research 24(8) (2010) 697–702.
[77]. A.G. Hassabo, Preparation, characterisation and utilization of some textile auxiliaries, El-Azhar University, Cairo, Egypt, 2005.
[78]. A.L. Mohamed, Acrylamide derivatives as additives to multifinishing formulations of cotton fabrics, Helwan University, Cairo, Egypt, 2005, p. 378.
[79]. M.H. Abo-Shosha, F.A. Nassar, Z. El-Sayed, A.G. Hassabo, Utilization of fatty acid/peg condensates as textile softeners, 3rd International Conference of Textile Research Division, NRC; Textile Processing: State of the Art & Future Developments, Cairo, Egypt, 2006, p. 369.

[80]. M.H. Abo-Shosha, F.A. Nassar, Z. El-Sayed, A.G. Hassabo, Preparation and characterizations of some fatty acid/polyethylene glycol condensates, Egyptian First International Conference in Chemistry: Chemistry for Human Needs In Developing Countries, Sharm El-Sheikh, Egypt, 2006.
[81]. A. Waly, M.M. Marie, N.Y. Abou-Zeid, M.A. El-Sheikh, A.L. Mohamed, Flame retarding, easy care finishing and dyeing of cellulosic textiles in one bath, Egy. J. Text. Polym. Sci. Technol. 12(2) (2008) 101–131.
[82]. F.A. Nassar, M.H. Abo-Shosha, K.M. Haggag, Z. El-Sayed, A.G. Hassabo, Utilization of some fatty acid/peg condensates as emulsifiers in kerosene paste pigment printing, 3rd International Conference of Textile Research Division, NRC; Textile Processing: State of the Art & Future Developments, Cairo, Egypt, 2006, pp. 359 – 368.
[83]. M.H. Abo-Shosha, F.A. Nassar, Z. El-Sayed, A.G. Hassabo, Preparation and characterizations of some fatty acid/polyethylene glycol condensates and utilization as softeners for cotton fabric, RJTA 13(2) (2009) 46–60.
[84]. A.G. Hassabo, Synthesis and deposition of functional nano-materials on natural fibres RWTH Aachen University, Germany, 2011, p. 154.
[85]. A.L. Mohamed, Changing the properties of natural fibres by coating and of synthetic fibres by infiltration, RWTH Aachen University, 2011, p. 251.
[86]. A.G. Hassabo, A.A. Nada, H.M. Ibrahim, N.Y. Abou-Zeid, Impregnation of silver nanoparticles into polysaccharide substrates and their properties, Carbohydrate Polymers 122 (2015) 343–350.
[87]. A.L. Mohamed, M.E. El-Naggar, T.I. Shaheen, A.G. Hassabo, Novel nano polymeric system containing biosynthesized core shell silver/silica nanoparticles for functionalization of cellulosic based material, Microsys. Technol. 22(5) (2016) 979–992.
[88]. A.G. Hassabo, M.E. El-Naggar, A.L. Mohamed, A.A. Hebeish, Development of multifunctional modified cotton fabric with tri-component nanoparticles of silver, copper and zinc oxide, Carbohydrate Polymers 210 (2019) 144–156.
[89]. A.G. Hassabo, A.L. Mohamed, A.A. Nada, N.Y.A. Zeid, Controlled release of drugs from cellulosic wound bandage using silica microsphere as drug encapsulator module, JAPS 5(12) (2015) 067–073.
[90]. A.A. Nada, A.G. Hassabo, H.M. Awad, W. Fayad, N.M. Shaffie, A.A. Sleem, N.Y.A. Zeid, Biomaterials based on essential fatty acids and carbohydrates for chronic wounds, JAPS 5(10 (Suppl 3)) (2015) 13–21.
[91]. H. Elmotasem, S.A. El-Marasy, A.L. Mohamed, Benzocaine mesoporous silica nanoparticles/bio polysaccharides-based hydrogels loaded cotton bandage as a platform for topical anesthesia, Results in Chemistry 5 (2023) 100830.
[92]. A.G. Hassabo, F. Saad, B.M. Hegazy, H. Elmorsy, N. Gamal, A. Sedik, H. Othman, Intelligent wound dressing textile fabric using various smart materials, Materials International 5(1) (2023) 1–23.
[93]. L. Chen, Y. Xie, X. Chen, H. Li, Y. Lu, H. Yu, D.J.I.J.o.B.M. Zheng, O-carboxymethyl chitosan in biomedicine: A review, (2024) 133465.
[94]. P. Lin, L. Liu, G. He, T. Zhang, M. Yang, J. Cai, L. Fan, S. Tao, Preparation and properties of carboxymethyl chitosan/oxidized hydroxyethyl cellulose hydrogel, Int J Biol Macromol 162 (2020) 1692–1698.
[95]. F. Zheng, R. Li, Q. He, K. Koral, J. Tao, L. Fan, R. Xiang, J. Ma, N. Wang, Y. Yin, Z. Huang, P. Xu, H. Xu, The electrostimulation and scar inhibition effect of chitosan/oxidized hydroxyethyl cellulose/reduced graphene oxide/asiaticoside liposome based hydrogel on peripheral nerve regeneration in vitro, Materials Science and Engineering: C 109 (2020) 110560.
[96]. F. Mohabatpour, Z. Yazdanpanah, S. Papagerakis, X. Chen, P. Papagerakis, Self-crosslinkable oxidized alginate-carboxymethyl chitosan hydrogels as an injectable cell carrier for in vitro dental enamel regeneration, Journal of Functional Biomaterials 13(2) (2022) 71.
[97]. N.M.B. Ladeira, C.L. Donnici, J.P. de Mesquita, F.V. Pereira, Preparation and characterization of hydrogels obtained from chitosan and carboxymethyl chitosan, Journal of Polymer Research 28(9) (2021) 335.
[98]. H. Zhao, N.D. Heindel, Determination of degree of substitution of formyl groups in polyaldehyde dextran by the hydroxylamine hydrochloride method, Pharmaceutical Research 8(3) (1991) 400–402.
[99]. L. Ma, Y. Tan, X. Chen, Y. Ran, Q. Tong, L. Tang, W. Su, X. Wang, X. Li, Injectable oxidized alginate/carboxylmethyl chitosan hydrogels functionalized with nanoparticles for wound repair, Carbohydrate Polymers 293 (2022) 119733.
[100]. Z. Wei, J. Zhao, Y.M. Chen, P. Zhang, Q. Zhang, Self-healing polysaccharide-based hydrogels as injectable carriers for neural stem cells, Scientific reports 6(1) (2016) 37841.
[101]. X. Liu, Y. Sun, J. Wang, Y. Kang, Z. Wang, W. Cao, J. Ye, C. Gao, A tough, antibacterial and antioxidant hydrogel dressing accelerates wound healing and suppresses hypertrophic scar formation in infected wounds, Bioactive Materials 34 (2024) 269–281.
[102]. D. Gago, M.C. Corvo, R. Chagas, L.M. Ferreira, I. Coelhoso, Protein adsorption performance of a novel functionalized cellulose-based polymer, Polymers 14(23) (2022) 5122.
[103]. D. Stan, E. Codrici, A.-M. Enciu, E. Olewnik-Kruszkowska, G. Gavril, L.L. Ruta, C. Moldovan, O. Brincoveanu, L.-A. Bocancia-Mateescu, A.-C. Mirica, Exploring the impact of alginate—PVA ratio and the addition of bioactive substances on the performance of hybrid hydrogel membranes as potential wound dressings, Gels 9(6) (2023) 476.
[104]. J.-p. Jeong, K. Kim, E. Oh, S. Park, S. Jung, Self-healing hydrogels with intrinsic antioxidant and antibacterial properties based on oxidized hydroxybutanoyl glycan and quaternized carboxymethyl chitosan for ph-responsive drug delivery, Gels 11(3) (2025) 169.
[105]. AOAC 991.20-1994(1996), Nitrogen (total) in milk. Kjeldahl methods, Association of Official Analytical Chemists,, Washington DC., 2000.
[106]. ASTM D 3590-89(1994)e1, Standard test methods for total kjeldahl nitrogen in water, 1994.

[107]. ASTM E 258 − 07 (Reapproved 2015), Total nitrogen in organic materials by modified kjeldahl method, Conshohocken, PA, USA., 2018.
[108]. A.L. Mohamed, M.A. El-Sheikh, A.I. Waly, Enhancement of flame retardancy and water repellency properties of cotton fabrics using silanol based nano composites, Carbohydrate Polymers 102 (2014) 727–737.
[109]. AATCC TM100-2019, Assessment of antimicrobial finishes on textile materials, Technical Manual Method American Association of Textile Chemists and Colorists, 2019.
[110]. A.H. Saputra, L. Qadhayna, A.B. Pitaloka, Synthesis and characterization of carboxymethyl cellulose (cmc) from water hyacinth using ethanol-isobutyl alcohol mixture as the solvents, International Journal of Chemical Engineering and Applications 5(1) (2014) 36.
[111]. R. Bai, H. Yong, X. Zhang, J. Liu, J. Liu, Structural characterization and protective effect of gallic acid grafted o-carboxymethyl chitosan against hydrogen peroxide-induced oxidative damage, International journal of biological macromolecules 143 (2020) 49–59.
[112]. Z. Emami, M. Ehsani, M. Zandi, R. Foudazi, Controlling alginate oxidation conditions for making alginate-gelatin hydrogels, Carbohydrate polymers 198 (2018) 509–517.
[113]. C. Mahmoudi, N. Tahraoui Douma, H. Mahmoudi, C.E. Iurciuc, M. Popa, M. Hamcerencu, C.V. Andrițoiu, Developing and characterizing a biocompatible hydrogel obtained by cross-linking gelatin with oxidized sodium alginate for potential biomedical applications, Polymers 16(22) (2024) 3143.
[114]. S.E. Samuel, T. Ghosh, A.D. Nayak, R. Deveswaran, B.V. Basavaraj, Exploring self-crosslinked hydrogel: Carboxymethyl chitosan and oxidized alginate for wound healing applications, Journal of Drug Delivery Science and Technology 97 (2024) 105746.
[115]. A.L. Mohamed, A.G. Hassabo, S. Shaarawy, A. Hebeish, Benign development of cotton with antibacterial activity and metal sorpability through introduction amino triazole moieties and agnps in cotton structure pre-treated with periodate, Carbohydrate Polymers 178 (2017) 251–259.
[116]. A.G. Hassabo, E.M. Reda, H. Ghazal, H.A. Othman, Synthesis of agnps and znonps using tea leaves extract and their utilization to improve dyeability, printability and functionality of cotton and wool fabrics, Inorg. Chem. Commun. 150 (2023) 110525.
[117]. S.P. Pasaribu, J. Kaban, M. Ginting, J. Silalahi, Preparation of in situ cross-linked n-maleoyl chitosan-oxidized sodium alginate hydrogels for drug delivery applications, Open Access Macedonian Journal of Medical Sciences 7(21) (2019) 3546.
[118]. H. Liao, H. Zhang, W. Chen, Differential physical, rheological, and biological properties of rapid in situ gelable hydrogels composed of oxidized alginate and gelatin derived from marine or porcine sources, Journal of Materials Science: Materials in Medicine 20 (2009) 1263–1271.
[119]. L. Zamora-Mendoza, S.N. Vispo, L. De Lima, J.R. Mora, A. Machado, F. Alexis, Hydrogel for the controlled delivery of bioactive components from extracts of eupatorium glutinosum lam. Leaves, Molecules 28(4) (2023) 1591.
[120]. H.P. Felgueiras, J.C. Antunes, M.C.L. Martins, M.A. Barbosa, Fundamentals of protein and cell interactions in biomaterials, Peptides and proteins as biomaterials for tissue regeneration and repair, Elsevier2018, pp. 1–27.
[121]. Y. Ramdhun, M. Mohanta, T. Arunachalam, R. Gupta, D. Verma, Bromelain-loaded polyvinyl alcohol–activated charcoal-based film for wound dressing applications, Macromolecular Research 31(5) (2023) 469–488.
[122]. L. Maeso, P.E. Antezana, A.G. Hvozda Arana, P.A. Evelson, G. Orive, M.F. Desimone, Progress in the use of hydrogels for antioxidant delivery in skin wounds, Pharmaceutics 16(4) (2024) 524.
[123]. K. Zouari Bouassida, S. Bardaa, M. Khimiri, T. Rebaii, S. Tounsi, L. Jlaiel, M. Trigui, Exploring the urtica dioica leaves hemostatic and wound-healing potential, BioMed research international 2017(1) (2017) 1047523.
[124]. R. Ogawa, Keloid and hypertrophic scars are the result of chronic inflammation in the reticular dermis, Int J Mol Sci 18(3) (2017).
[125]. A.G. Morena, S. Pérez-Rafael, T. Tzanov, Lignin-based nanoparticles as both structural and active elements in self-assembling and self-healing multifunctional hydrogels for chronic wound management, Pharmaceutics 14(12) (2022) 2658.